The Pennsylvania State University

The Graduate School

College of Earth and Mineral Sciences/ College of Engineering

POLY-ETHYLENEDIOXYTHIOPHENE (PEDOT) CONFORMALLY COATED ON ALIGNED CARBON NANOTUBE ARRAYS FOR SUPERCAPACITOR ELECTRODES

A Thesis in

Materials Science and Engineering

by

Suppanat Kosolwattana

Submitted in Partial Fulfillment
of the Requirements
for the Degree of

Master of Science

August 2013

The thesis of Suppanat Kosolwattana was received and approved* by the following:

Qiming Zhang
Distinguished Professor of Electrical Engineering and Material Science and Engineering
Thesis Advisor

Michael Hickner
Assistant Professor of Material Science and Engineering

Clive A. Randall
Professor of Materials Science and Engineering

Joan M. Redwing
Professor of Materials Science and Engineering
Chair, Intercollege Graduate Degree Program in Materials Science and Engineering

*Signatures on file in the Graduate School

Abstract

Symmetric supercapacitors with aligned carbon nanotube (A-CNT) electrodes have showed a promising performance as an energy storage device. A-CNTs morphology presents high surface area for forming double layer charge storage with electrolyte ions. In this study, 3,4-ethylenedioxylthiophene (PEDOT) conducting polymer is selected to coat on A-CNTs electrodes to provide pseudo-capacitance from fast faradic reactions with electrolyte ions. Ionic liquid 1-ethyl-3-methylimidazolium tetrafloroborate ($EMIBF_4$) in propylene carbonate (PC) is utilized as the electrolyte in chapter 3 to analyze the performance of coating material. Then, two other ionic liquids, N-Butyl-N-methylpyrrolidinium bis(trifluoromethanesulfonyl) imide ($Pyr_{14}TFSI$) and 1-ethyl-3-methylimidazolium bis(trifluoromethanesulfonyl) imide (EMITFSI) are introduced to find the suitable electrolyte for new coated electrodes. The performance of the device, such as power density, energy density, capacitance and conductivity, are investigated by using impedance spectroscopy, cyclic voltammetry, and galvanostatic charge-discharge experiment. Electrode composition, surface area and morphology are determined from scanning electron microscopy (SEM) and transmission electron microscopy (TEM). The conducting polymer coated on ACNTs is expected to increase surface area, produce pseudo-capacitance, and support the electrode structure. These improvements will lead to high performance supercapacitor.

TABLE OF CONTENTS

LIST OF FIGURES

LIST OF TABLES

ACKNOWLEDGEMENTS

First, I would like to thank my adivisor Dr. Qiming Zhang for giving me a lot of opportunity to learn in this study. I also would like to thank Dr. Hickner and Dr. Randall for serving as my thesis committee. Then, I would like to thank my colleagues (Mehdi and Yue) who helped me conduct my study for a whole year. I would like to thank Joshua Michalenko who help me proofread my entire thesis. I would like to thank my Thai friends in MatSE department for the supports (Jess, Wut and especially Nim who helped me prepare my thesis defense.) I would like to thank the ministry of science and technology of Thailand for my scholarship. Finally, I would like to thank my friends and family and others that I do not mention for the supports along the way of my study.

Chapter 1

Introduction

1.1 Supercapacitors

Capacitors are electronic components that can store electrostatic energy from dielectric polarization between two electrodes in an applied electric field. The capacitance of a parallel plate capacitor can be calculated by equation [1]:

$$C = \varepsilon\varepsilon_0 A/d \qquad (1)$$

Where C is capacitance, A is surface area of electrodes, d is the separation distance of the two electrodes, ε is dielectric constant, and ε_0 is the permittivity of free space = 8.85×10^{-12} F/m. Supercapacitors are capacitors that have an ionic electrolyte as the dielectric media and ions from the electrolyte can form electrochemical double layers to store charge at the electrodes (Figure 1.1) [2]. There are two mechanisms to generate capacitance in a supercapacitor. The first mechanism is the Electrochemical Double Layer Capacitance (EDLC) which has no faradic reactions involved. Another mechanism is called pseudo-capacitance which is a fast faradic reaction that electrodes reversibly exchange electrons with electrolyte ions [3]. The pseudo-capacitance will be discussed in more detail in metal oxides and conducting polymer sections. Supercapacitor is a useful energy storage device in many electronic applications such as memory backup, cell phones, and hybrid electric vehicles [4]. Form the Ragone plot (Figure 1.2) [5], supacapacitor can provide high power density and fair energy density compared to batteries and other energy storage devices. As a simple series RC circuit model (Figure 1.3), energy density and power density can be estimated as equation (2) and (3) [6]. From these equations, high

specific capacitance (C), high operating voltage (V), and low equivalent series resistance (ESR) are required to optimize supercapacitor performance.

$$E = \frac{1}{2}CV^2 \qquad (2)$$

$$P = \frac{V^2}{4 \times ESR} \qquad (3)$$

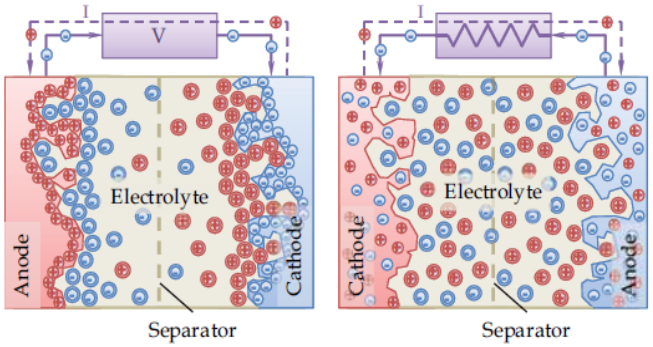

Figure 1.1: Supercapacitor charge-discharge model [2]

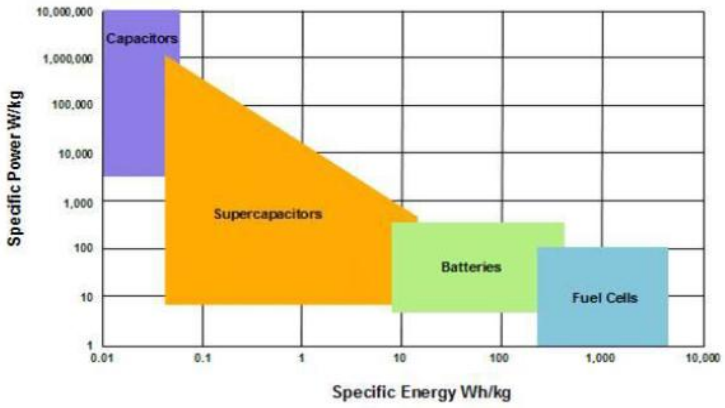

Figure 1.2: Ragone plot of energy storage devices [5]

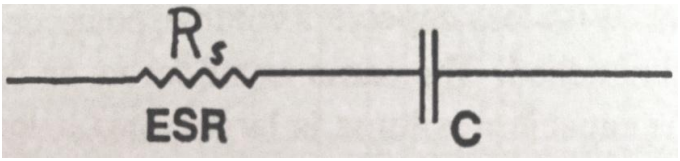

Figure 1.3: Series RC circuit [6]

In this thesis, only symmetric supercapacitors which have identical anode and cathode materials are discussed. For symmetric supercapacitors, capacitances of both anode and cathode

are also assumed to be similar and each electrode has double layer capacitance. Therefore, like 2 capacitors connected in series, the capacitance of each electrode (C_1) is 2 times of cell capacitance (C_{total}) following series capacitance equation (4) [7]:

$$\frac{1}{C_{total}} = \frac{1}{C_1} + \frac{1}{C_1} \quad (4), \quad \text{for 2 identical } C_1 \text{ in series:} \quad C_1 = 2C_{total}$$

For specific capacitance is the capacitance per weight of one electrode, then:

$$C_{sp} = C_1/M_{electrode} = 2C_{total}/(M_{total}/2) \quad (5) \qquad \text{so,} \qquad C_{sp} = 4C_{total} \quad (6)$$

Where C_{total} in equation (6) is a per weight value.

1.2 Electrode materials

The electrode is a key component to making supercapacitors. High performance electrodes should provide very high specific capacitance that contributes to the energy density of the device. The technique to improve capacitance will be discussed later in this study. Also, electrodes should have a stable mechanical and chemical structure, high surface area, high ion accessibility, and low cost of production. There are many types of electrodes for supercapacitors which are discussed in the next section

.

1.2.1 Carbon based electrodes

Carbon based electrodes such as activated carbon, carbon nanotube (CNTs) and graphene have very large surface area structure could provide more specific capacitance [8-10]. Table 1.1 compares the properties of each carbon based electrode [11]. CNTs generally have a low volumetric capacitance. In order to improve CNT electrode performance, the experimental methods to organize structures and package aliments are intensively studied. Recently, Futaba et

al. [12] successfully used a liquid-induced collapse method to pack or densify CNT forests to high volumetric electrodes (Figure 1.4). Similarly, Wardle's research group from the Massachusetts Institute of Technology (MIT) [13] successfully found another method that utilizes biaxial mechanical forces for CNT forest densification. Because our research group has been collaborating with Wardle's group, the samples and this densification technique are utilized for this thesis study. The fabrication details for densifing CNTs will be explained in chapter 2. Not only do CNT forest electrodes have a high volumetric capacitance, but these CNT forest also has alignment direction which allows for faster ion accessibility than random aliment CNTs (Figure 1.5) [14]. Energy density and power density will be greatly improved by utilizing aligned carbon nanotube array (A-CNT) electrodes.

Material	Carbon onions	Carbon nanotubes	Graphene	Activated carbon	Carbide derived carbon	Templated carbon
Dimensionality	0-D	1-D	2-D	3-D	3-D	3-D
Conductivity	High	High	High	Low	Moderate	Low
Volumetric Capacitance	Low	Low	Moderate	High	High	Low
Cost	High	High	Moderate	Low	Moderate	High
Structure	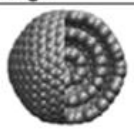	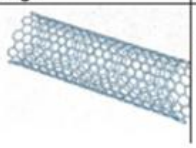	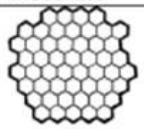	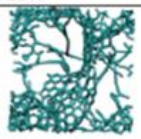	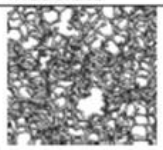	

Table 1.1: Carbon based electrode properties [11]

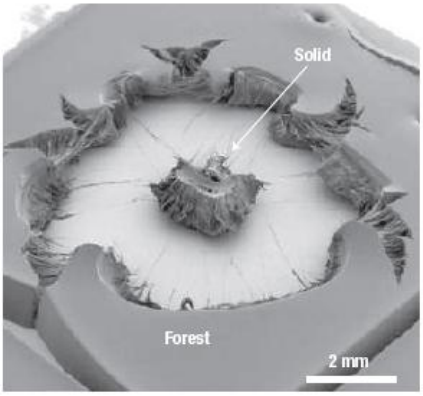

Figure 1.4: CNT forrest densification with the liquid-induced collapsing method [12]

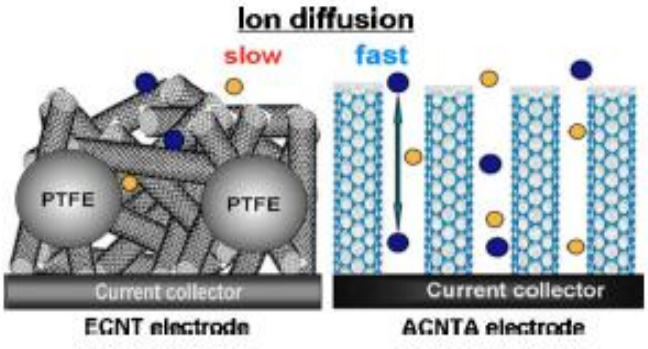

Figure 1.5: Schematic comparison of ion diffusion process in align carbon nanotubes and random carbon nanotube forests[14]

1.2.2 Metal oxides

Certain metal oxides can be used for supercapacitor electrode and can provide very high specific capacitance values with pseudo-capacitive reactions. The best metal oxide electrode is RuO_2 which can provide capacitance values up to around 1200 F/g [15]. However, RuO_2 is not abundant cause a very high cost of production. A common matal oxide for supercapacitors is MnO_2 whose can fast faradic reaction in Figure 1.6 produces a fair amount of pseudo-capacitance of about 100-400 F/g [16]. There are some limitations in using metal oxides such as low conductivity and stiff rigid metal oxide structure [9,17]. These types of materials could be good candidates for future studies.

$$MnO_2 + C^+ + e^- \leftrightarrow MnOOC$$

Figure 1.6: Fast faradic reaction of metal oxide in supercapacitors [16]

1.2.3 Conducting polymers (CPs)

Conducting polymer is another interesting electrode type which could provide fairly high pseudo-capacitance, flexible structure, and low cost of production [18]. There are some common

conducting polymers that have been intensively study for supercapacitors. For example, poly aniline (PANI), polyprrole (PPy) and PEDOT (3,4-ethylenedioxythophene) as shown in Figure 1.7. Disadvantages of using conducting polymers are that polymers are easily decomposed so polymers can tolerate low potential and also, polymers slow ion diffusion due to a bulky structure [19].

In this thesis study, PEDOT is selected to cooperate with A-CNT electrodes. First, PEDOT has a flexible structure, high conductivity and a fair capacitance of around 210 F/g [20]. Also, PEDOT has more chemical stability than most other conducting polymers when cyclic voltammetry curves are compared. Last but not least, PEDOT can be adjusted to favor both cathode and anode by being n-doped and p-doped electrodes (see reaction in Figure 1.8) [19, 21].

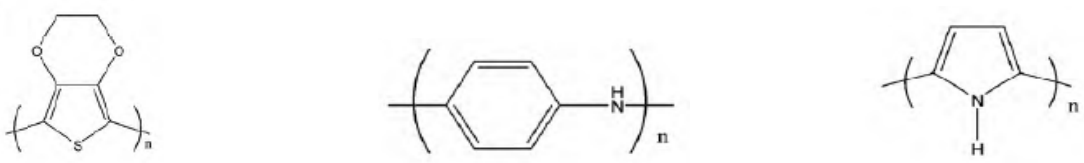

Figure 1.7: Structure of PEDOT (left), PPy (middle) and PANI (right) [19]

$$Cp \rightarrow Cp^{n+}(A^-)_n + ne^- \quad (p\text{-doping})$$
$$Cp + ne^- \rightarrow (C^+)_n Cp^{n-} \quad (n\text{-doping})$$

Figure 1.8: Fast faradic reaction of conducting polymer (p-doping and n-doping) [19]

1.2.4 Composite electrodes

Combinations of each type of electrode could support the electrochemical performance of supercapacitors. In this thesis study, PEDOT is conformally coated on vertically A-CNTs which creates a very unique structure. The conducting polymer coating causes higher volumetric capacitance in the electrodes with densification process while still maintaining empty space

between the A-CNTs which allows for fast ion diffusion [22]. Moreover, the conductive properties of PEDOT contribute to high power with during the drifing process. The performances of composite PEDOT supercapacitors in literatures were collected in Table 1.2 for comparison with our PEDOT conformally coated on A-CNT supercapacitors.

Sample	Electrolyte	Voltage	sp capacitance	max Energy Wh/kg	max Power kW/kg
Pedot_F-SWNTs	1 M KCl	1.0	170-210 F/g	-	-
80%-Pedot_MCNTs	1M TEABF4/AN	1.5	100 F/g	-	-
80%-Pedot_MCNTs/carbon	1 M H2SO4	1.8	120 F/g	-	-
92%-Pedot_g-MCNTs	1 M LiClO4	1.0	81 F/g	11.3	5
30%-Pedot-RuORuCN_MCNTs	1 M H2SO4	1.0	123 F/g	13.6	9.2
70%-Pedot_MCNTs	1 M TEABF4/AN	1.2	60 F/g	-	-
70%-Pedot-PSS_SWNTs	1 M NaNO3	1.0	85 F/g	2.8	1.11

Table 1.2: PEDOT composite properties comparison [23-28]

1.3 Electrolytes

The most common electrolyte that is generally used for commercial supercapacitors is Et_4NBF_4 or $TEABF_4$ (tetraethylammonium tetrafluoroborate) salt in molecular liquid [29]. However, the use of ammonium salt in supercapacitors results in poor performance of the device. [30]. Therefore, ionic liquids are introduced for supercapacitors to solve these issues.

1.3.1 Ionic liquids (ILs)

Ionic liquids are ionic molten salts composed of asymmetric structures of cations and charge delocalized anions [31]. ILs have been useful in electrochemical devices due to their

unique properties. Non-volatility and non-flammability are the first concern properties to use ILs for a safe application. Moreover, other properties of ILs such as wide electrochemical window, high conductivity, and excellent thermal stability also enhance device performance. ILs properties have been collected as shown in Table 1.3.

Ue et al. reported that $EMIBF_4$ (1-ethyl-3-methylimidazolium tetrafluoroborate) has the overall high performance as an electrolyte for supercapacitors because of high conductivity and low viscosity compared to other EMI^+ ILs [32]. Another interesting IL is $Pyr_{14}TFSI$ (N-Butyl-N-methylpyrrolidinium bis(trifluoromethanesulfonyl) imide). This IL is a bit lower conductivity and higher viscosity than $EMIBF_4$. However, this electrolyte can operate at very high voltage and on wide range temperature compared to some other ILs [33]. The electrochemical window of $Pyr_{14}TFSI$ is approximately 6.0 V. Some research group has intensively studied on this IL [34-35], especially for asymmetric and hybrid supercapacitors. The amazing results from $Pyr_{14}TFSI$ performance show the very stable long life cycles that the capacity dropped only 5-10% for 14000 cycles in Hybrid AC/pMeT hybrid supercapacitors and for 40000 cycle of general carbon-carbon supercapacitor.

Ionic liquids	T_m (^oC)	η (mPas)	σ (mS/cm)	EW (V)
$EMIBF_4$	15	32	13.6	4.5
EMIF.2.3HF	-90	5	100	4.0
EMITF	-10	43	9.3	4.3
EMITFSI	-15	28	9.3	4.6
$BMIBF_4$	n/a	112	1.7	4.7
BMITFSI	n/a	52	3.9	4.8
$Et_4NFPFSI$	6	104	1.6	5.96
$N_{22.2(102)}TFSI$	7	101	1.77	5.73
$N_{22.2(102)}FSI$	15	81	2.77	5.41
$S_{221}TFSI$	-22.6	36	5.80	3.9
$S_{123}TFSI$	<-60	39	4.70	4.0
OEPZ-TFSI	<-60	41.2	3.31	4.4
OMMPZ-TFSI	<-60	73.0	2.45	4.4
PIP_3TFSI	12	149	1.5	6.02
$Pyr_{13}TFSI$	11	60	3.8	5.89
$Pyr_{14}TFSI$	-18	100	2.48	5.90

$Pyr_{1(201)}TFSI$	n/a	62	2.43	3.7
$Pyr_{1(101)}TFSI$	n/a	40.7	5.5	n/a
$Pyr_{13}FPFSI$	n/a	56	3.5	5.98
$Pyr_{14}BETI$	8.9	350	0.42	n/a
$Pyr_{14}IM_4$	n/a	560	0.28	n/a
$Pyr_{14}TF$	3	158	2.0	5.0
$Pyr_{14}FSI$	n/a	53.2	6.19	n/a
$Pyr_{13}FSI$	-17	45	7.4	5.0
$Pyr_{1(101)}FSI$	n/a	28.5	10.3	n/a

Table 1.3: Ionic liquids reported in literature [32, 36-44]

* Highlighted ILs are used in this study

ILs which has very wide electrochemical window usually posses the property of high viscosity. Therefore, in this practical usage, ILs still have to mix with molecular liquids such as acetonitrile (AN) and propylene carbonate (PC) (See Table 4) [45] in order to posses properties such as high conductivity and low viscosity at ambient temperature. In addition, PC solvent was selected for this study not only overall suitable properties for supercapacitors listed in Table 1.4, but PC also has a wide electrochemical window (from -2.2 to 2.3 V or about 4.5 V) [6]. Therefore, the experimental operating voltage could be optimized.

Solvent	Bp.	Mp.	Permitivity	Viscosity (25 °C)
Propylene carbonate	241°C	-55°C	65	2.8 mPa·s
Dimethylsulfoxide	189°C	18.5°C	29.8	1.996 mPa·s
N, N dimethylformamide	153°C	-61°C	30.9	0.92 mPa·s
Ethylene carbonate	260°C	37°C	95	1.92 mPa·s
Diethyl carbonate	128°C	-48°C	-	0.795 mPa·s
Acetonitrile	82°C	-45°C	38	0.369 mPa·s
Sulfolane	285	26	14.8	10 mPa·s
γ-butyrolactone	204	-44	42	1.7 mPa·s

Table 1.4: Properties of macular liquid solvents [45]

1.3.2 Ion transport

In this study, the ACNT electrodes are expected to improve the diffusion process by providing uniform ion channels. The conducting polymer coating is not only expected to enhance capacitance but also expected to provide more conductive element to induce more efficient ion movement. Besides, the study of this new electrolyte could help to find suitable media to maximize supercapacitor performance. The overall expected ion transport system is schematically shown as Figure 1.9 [46].

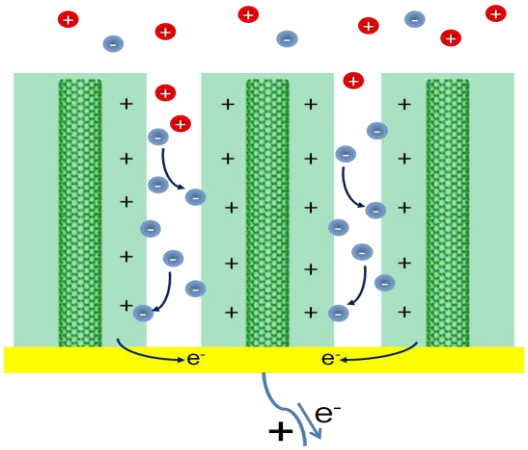

Figure 1.9: Schematic of ion transport in PEDOT/A-CNT electrodes [46]

1.3.3 Electrochemical window

The electrochemical window limits the performance of the device by decomposition of te electrode or electrolytes if voltages outside of the window are used. Thus, electrolytes which have wide electrochemical windows and high conductivity are the best candidates for supercapacitor applications.

The electrochemical window of ILs depends on structure stability of the cations and anions. Ionic liquids that have wide electrochemical windows mean that both cations and anions

require very high potentials to decompose. For the anion, a decomposition reaction usually is an oxidation reaction in that anions will start to lose an electron or charge is potential is out of the range of the chemical window. Anions that have a stable structure which usually contain electron withdrawing groups such as fluorine and symmetric structures to stabilize the electron especially at the center atom of the anion which make it difficult to lose electrons. The order of wide chemical window to narrower chemical window of the anions used is FAP^->PF_6^->BF_4^-> NTf_2 (or TFSI)$^-$> OTf^- > $MeSO_4^-$ and NO_3^- (Figure 1.10) [47].

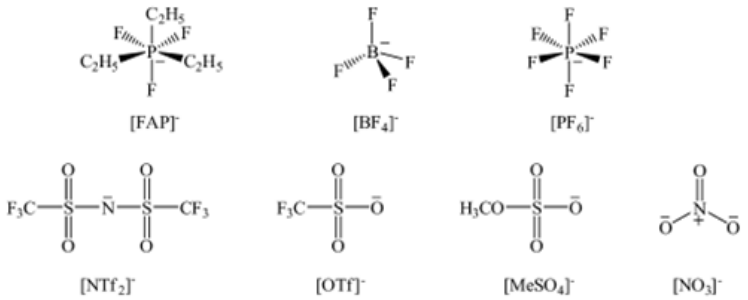

Figure 1.10: Structure of anions [47]

For cations, reduction reactions control the decomposition mechanism when the potential is outside of the chemical window in which cations start to accept electrons. A similar analogy to anions, stable structure cations usually have an electron donating group such as methyl to make center or active atoms in cations difficult to accept more electrons. The trend of stable structures of cations, from most to least stable is quaternary ammonium (c) = phophonium (f) > 1,2,3-trialkyl-imidazole (b) = morpholinium (d) >1,3-dialkyl-imidazole (a) > sulfonium (e) > pylidine (g) as shown in Figure 1.11 [48]. The simplest structure as quaternary ammonium, which is also the most stable structure. Compare this to morpholinium which has an ether group to withdraw electrons and is less stable. Pyrrolidinium, or Pyr^+,is one of the quaternary ammonium ions with

ring structure. Therefore, Pyrrolidinium ionic liquids usually demonstrate high electrochemical windows.

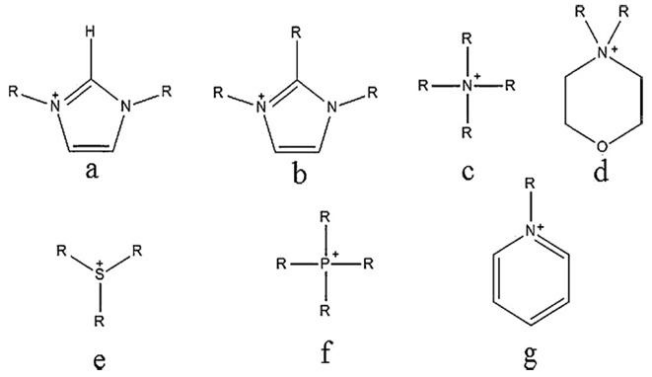

Figure 1.11: Structures of cations [48]

In this thesis, $EMIBF_4$/PC mixture showed very high performance in my group's research[22]. This mixture was used as a reference to compare the performance of coated electrodes in chapter 3. For chapter 4, EMITFSI and Pyr14TFSI were introduced to analyze the effects of different anions ($TFSI^-$ andBF_4^-) and cations (EMI^+ and Pyr_{14}^+) in the new coated electrode supercapacitors. The effects of PC molecular liquid with EMITFSI and Pyr_{14}TFSI were discussed in this chapter as well.

Chapter 2

Experimental Methods and Characterizations

2.1 Synthesis of electrode

In this section, all the electrode samples for this thesis study (both coated and uncoated CNTs) are synthesized and supplied by students and researchers from Dr. Wardle's group at the Massachusetts Institute of Technology (MIT)[13,49]. Multiwalled carbon nanotubes (MCNTs) were synthesized via thermal catalytic chemical vapor deposition with a thin catalyst layer of Fe/Al_2O_3 at 750 ^oC. The aligned MCNTs arrays growth rate was approximately 2 μm/s. The as-grown CNT forests had a 1% volume fraction (Vf) with densities of 10^9-10^{10} CNTs/cm^3. The MCNTs (with 3-5 walls) had an average diameter of approximately 8 nm and the spacing between the aligned MCNTs (center to center) was approximately 80 nm (Figure 2.1a). Next, the as grown A-CNT forests were conformally deposited with the conducting polymer poly(ethylenedioxythiophene) (PEDOT) via an oxidative chemical vapor deposition process (Figure 2.1b). The coating process started with an iron chloride oxidizing agent sublimation into the CNT array. Then, CNTs with the oxidant were exposed to a vapor of EDOT monomer. Usually, EDOT was polymerized for 30 minutes including 5 minutes of oxidant sublimation. However, to obtain 8 times the coating thickness for the study, the coating process time was also multiplied by 8 times. PEDOT deposited on CNT forests at a temperature of 70 ^oC and a pressure of 50 mTorr and 8 nm thickness of PEDOT coating was obtained. Excessive amount of oxidizing agent were rinsed out of the sample with isopropyl alcohol. The morphology image of coated and uncoated ACNT was acquired with transmission electron microscopy (TEM) and scanning electron microscopy (SEM) as shown in Figure 2.2 and Figure 2.3 respectively. For high volume

fraction CNT fabrication, a mechanical biaxial densification process in two orthogonal directions was applied to vary inter-tube spacing of the CNT array (Figure 2.4) [13]. The 1% and 5% volume fraction arrays of coated and uncoated CNTs were obtained and compared in this study.

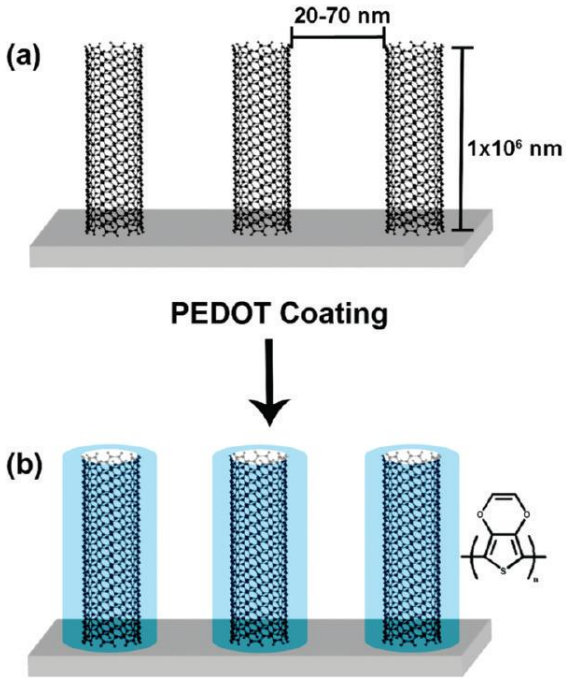

Figure 2.1: a) A-CNT arrays, b) PEDOT conformally coated on A-CNT arrays [49]

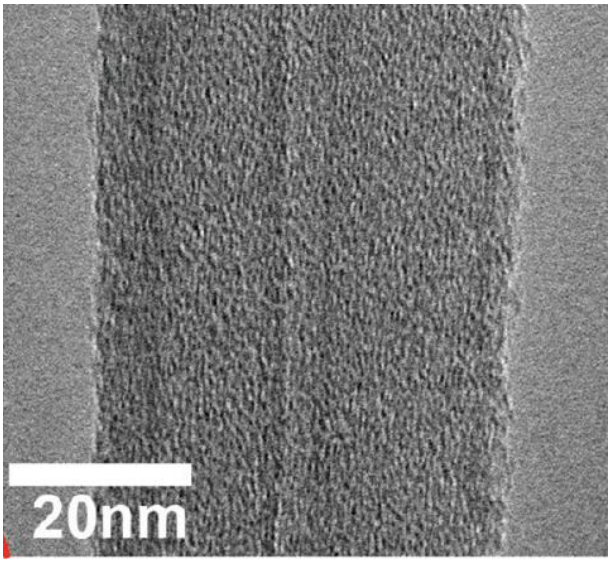

Figure 2.2: TEM image of A-CNT after coated with PEDOT [49]

Figure 2.3: SEM image of PEDOT-ACNT forest morphology (colorized with Adobe photoshop)

Figure 2.4: Biaxial mechanical densification of ACNT arrays [13]

2.2 Fabrication of the device [29, 50]

For Chapter 3, 200 micron thickness coated and uncoated A-CNT arrays at 1% and 5% were utilized for symmetric supercapacitor electrodes. A porous paper around 8 microns was provided as a separator. 3 M of EMI-BF_4/PC mixture was studied as electrolyte. A gold sheet on a stainless steel plate was pressed to each A-CNT electrode as a current collector. A whole cell from A-CNT cathode to A-CNT anode had a dimension of 0.2 cm x 0.2 cm square cross section

and 0.04 cm thickness. For Chapter 4, only 5% coated A-CNT arrays were applied for electrodes. Three pure ionic liquids $EMIBF_4$, EMITFSI, $Pyr_{14}TFSI$, 1 M of EMITFSI/PC and 1M of $Pyr_{14}TFSI$/PC were combined in the cell for use as the electrolyte.

2.3 Instruments and Characterizations [29, 50]

2.3.1 Cyclic voltammetry (CV)

Cyclic voltammetry or CV is a plot between current and potential to indicate the electrochemical behaviors such redox reactions, electrochemical windows and specific capacitance of a system. Cyclic voltammetry was characterized by using a Princeton Applied Research PARSTAT 2273 potentiostat. In Chapter 3, 1% and 5% coated and uncoated A-CNT cells generated CV curves at different scan rates (20, 50, and 100 mV/s) with a maximum voltage of 2.0 V. In Chapter 4, CV curves of 5% coated ACNT in a three electrode system (compared with an Ag standard electrode) with different ionic liquids ($EMIBF_4$, EMITFSI, and $Pyr_{14}TFSI$) were additionally measured to analyze electrochemical windows. CV curves of EMITFSI/PC and $Pyr_{14}TFSI$/PC at 1 M were also measured to analyze electrochemical behaviors from the effect of the solvent.

2.3.2 Galvanostatic charge-discharge

The galvanostatic curve is a plot between potential of charge-discharge time in each cycle. It can be calculated for specific capacitance, IR drop, power density and energy density. Galvanostatic curves of each samples in chapter 3 and 4 were also investigated by a Princeton Applied Research Versastat 4 potentiostat at different discharge rates (0.5, 1, 2.5, 5 and 10 A/g) and a maximum voltage of 2.0 V.

2.3.3 Electrochemical Impedance Spectroscopy (EIS)

EIS is a characterization technique containing real and imaginary impedance values at each frequency to indicate equivalent electronic circuits and internal resistance. The plot between real and imaginary impedance is called Nyquist plot. In this thesis, EIS of all electrode and electrolyte samples was operated with the same Princeton Applied Research PARSTAT 2273 potentiostat over a frequency range from 10 mHz to 1 MHz.

2.3.4 Capacitance Retention

Capacitance retention is a repeated test of Galvanostatic or CV curves to determine the stability of the device after running in many large cycles. Percent of generated capacitance compared to initial capacitance of each electrode and electrolyte samples in 1000 cycles were collected.

2.3.5 Coulombic Efficiency

Coulombic efficiency is a ratio or percent of the output or discharged energy and the input or charged energy to determine how good an application can store energy in one cycle. High performance supercapacitors should provide high coulombic efficiency or less loss of energy in each charge-discharge cycle. Coulombic efficiency can be calculated and interpreted from CV curves, galvanostatic curves and EIS.

2.4 Equations and Calculations [50]

2.4.1 Gravimetric capacitance

$$C = \frac{4I}{M\frac{dV}{dt}} \qquad (1)$$

Where I is the discharge current, M is the active material mass from both electrodes, and dV/dt is the slope of the galvanostatic discharge curve after the IR drop or scan rates in the CV curves. The volumetric capacitance values were then calculated by multiplying density of the samples to the gravimetric values.

2.4.2 Energy density

$$E = \frac{1}{8}C(V)^2 \qquad (2)$$

Where V is the maximum voltage and C is the specific capacitance.

2.4.3 Power density

$$P = \frac{(V)^2}{4ESR} \qquad (3) \qquad \text{and} \qquad ESR = \frac{\Delta V}{\Delta I} \qquad (4)$$

Where ESR is the equivalent series resistance, ΔV is the voltage drop or IR drop and ΔI is the current switched between charge and discharge.

2.4.4 Real and imaginary capacitance

$$C'(\omega) = \frac{-Z''}{\omega|Z(\omega)|^2} \quad (5) \quad \text{and} \quad C''(\omega) = \frac{-Z'}{\omega|Z(\omega)|^2} \quad (6)$$

Where Z' is the real impedance, Z'' is the imaginary impedance, and ω is the angular frequency. Also, $|Z(\omega)|^2 = Z'^2 + Z''^2$

2.4.5 Coulombic efficiency and loss tangent [6]

Coulombic efficiency (Eff) = $C_{discharge}/C_{charge}$

Also Coulombic efficiency (Eff) = 1 - loss

From CV and Galvanostatic, loss = the loop area in QV curves

From EIS, loss (tanδ) = $\frac{C''}{C'}$

Chapter 3

Results and Discussion: Electrodes

In this chapter, four electrode samples: 1% volume fraction uncoated aligned carbon nanotubes (1% A-CNTs), 5% volume fraction uncoated aligned carbon nanotubes (5% A-CNTs), 1% volume fraction PEDOT coated on aligned carbon nanotubes (1% PEDOT/A-CNTs) and 5% volume fraction PEDOT coated on aligned carbon nanotubes (5% PEDOT/A-CNTs) were composed in a symmetric supercapacitor cell with 3M of $EMIBF_4$/PC electrolytes and their energy storage performances were compared. First of all, cyclic voltammograms or CV curves of each sample were characterized to determine the optimal electrochemical window to stably operate devices. Capacitance values were also estimated from the CV curves. Next, energy density, power density, IR voltage drop, and specific capacitance performances of each cell were calculated from the galvanostatic charge-discharge test. Then, ion transport behaviors in each cell were analyzed with electrochemical impedance spectroscopy (EIS). Finally, performance stability of the devices after 1000 cycles was collected. The best electrode candidate for the next study in the following chapter can be concluded from these characterizations.

3.1 Electrochemical Window (EW) and Cyclic Voltammetry (CV) : Electrodes

Electrochemical window is the most important property to be characterized because the optimal operating voltage of a supercapacitor cell corresponds to the maximum energy density a cell can generate as in equation (1) in chapter 1. In the case of supercapacitor devices in which there are no real faradic reactions involved, the limitation of operating voltage comes from deformation and decomposition voltages of electrodes and electrolytes. From chapter 1, the

electrochemical window of $EMIBF_4$ and PC are both 4.5 V. Also, from the previous study [51], A-CNT electrodes have been proved to be able to operate at very high voltage up to 4 V with $EMIBF_4$/PC electrolytes. The difference in this study and the previous study is the lower limiting operating voltage of the electrode with the PEDOT coating. Conducting polymers usually cannot tolerate high voltages because the polymer structure generate too high of strain leading to deformation and then malfunction [23]. Also, the functional groups on polymer chains can interact with electrolyte species at certain potentials. Therefore, the electrochemical window of 5% PEDOT/A-CNT symmetric cell with $EMIBF_4$ was determined with cyclic voltammogram or current-voltage (CV) curves from 0 to 3.5 V as shown in Figure 3.1. An ideal shape of a CV curve for a stable supercapacitor is rectangular a hysteresis. Any peaks and bumps appeared on CV indicate some reactions occurred in the system. CV curves of PEDOT/A-CNT are steady up to 2-2.2 V (black line in Figure 3.1) and then reaction bumps start to appear beyond those voltages. In literatures [23,27-28], operating voltage of PEDOT supercapacitor is limited to around 1.2 V due to structure deformation and aqueous solution potential. However, the conformal coating of PEDOT on aligned nanotube structure provides stable operating device at higher voltage than other conducting polymer electrode systems. PEDOT coating deformation around the tubes will not disrupt the electric conduction paths of CNTs [46], so electrodes can still exhibit capacitance behavior with less disturbing of mechanical deformation. PC solvent addition to the ionic liquid also shows no significant effect on the operating voltage (Figure 3.2). Consequently, the optimal operating voltage at 2 V was selected to apply for comparison in this study.

Then, the CV curves of each electrode sample have been characterized at scan rate 100 mV/s and operating voltage 0-2 V with 3M of $EMIBF_4$/PC as shown in Figure 3.3. Both uncoated 1% A-CNT and 5% A-CNT shows a little more ideal rectangular CV curves than

coated PEDOT/A-CNT samples due to the high stable voltage of pure A-CNT electrodes. However, the current, which corresponds to capacitance as equation (1) in chapter 2, of PEDOT/A-CNT cells are higher than uncoated A-CNT cells. 1% and 5% PEDOT/A-CNT have gravimetric specific capacitance 214.5 F/g and 201.4 F/g while uncoated 1% and 5% A-CNT generate specific capacitance 104.4 F/g and 96.7 F/g respectively. This result shows that PEDOT coating has a significant contribution to capacitance. PEDOT not only provides more surface area for EDL capacitance but also performs pseudo-capacitive mechanism on A-CNT electrodes. Therefore, PEDOT coating electrodes should be a good candidate for future supercapacitor devices.

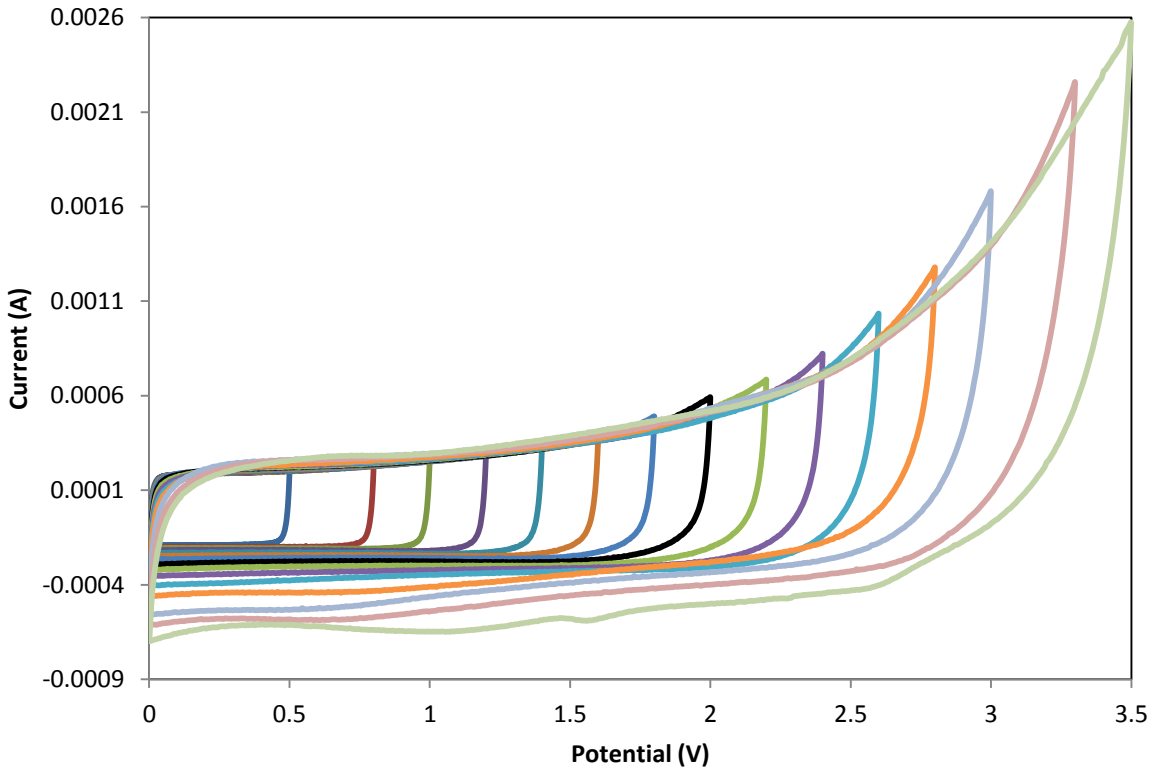

Figure 3.1: CV curves of PEDOT/ACNT with $EMIBF_4$ illustrated electrochemical widow of the cell

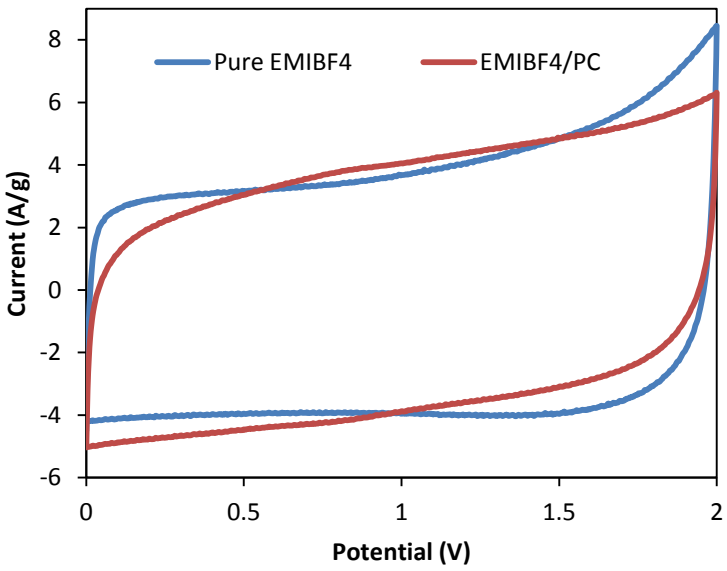

Figure 3.2: CV curves of 5% PEDOT/A-CNT with and without PC in the $EMIBF_4$ electrolyte

The gravimetric specific capacitance values of 1% volume fraction electrodes are higher than 5% volume fraction electrodes because more empty space in 1% electrodes allows more ions access for capacitive behaviors [51,52,54]. These gravimetric values do not exactly interpret the real performance of electrodes. The gravimetric capacitance values are calculated based on only active materials. In the real application, the empty space are filled with electrolyte, then the capacitance of the whole cell per weight includes electrolyte will become very low. The high volume fraction electrodes could effectively contribute more capacitance for the cell in the same size. Therefore, volumetric specific capacitance values are determined to illustrate more meaningful information of electrodes as shown in Figure 3.4. 1% and 5% PEDOT/A-CNT have volumetric specific capacitance 12.8 F/cm^3 and 83.9 F/cm^3 while uncoated 1% and 5% A-CNT generate specific capacitance 3.8 F/cm^3 and 18.1 F/cm^3 respectively. These results indicate much important role of high volume fraction electrodes. Both 5% coated and uncoated electrodes contribute higher capacitance compared to 1% volume fraction electrodes in the same volume

spaces. Thus, the contributions from both high volume fraction and PEDOT coating lead 5% PEDOT/A-CNT to show the highest energy storage performance.

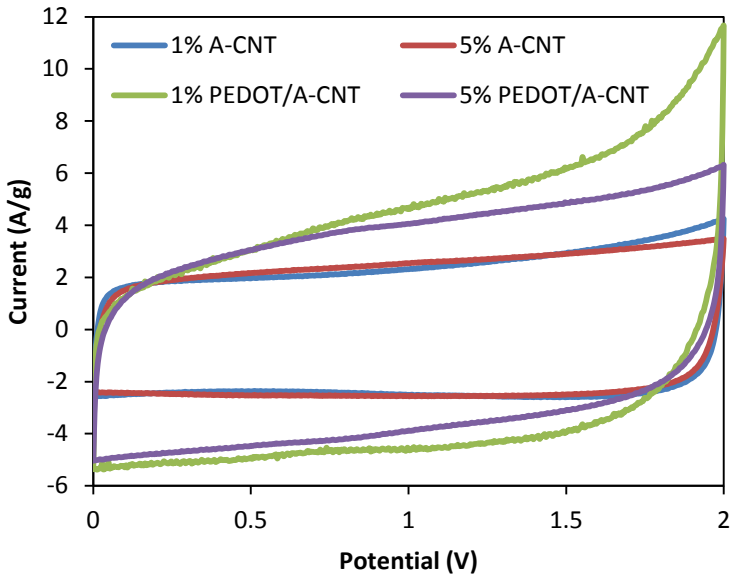

Figure 3.3: Gravimetric CV curves of supercapacitor cells of each kind of electrodes

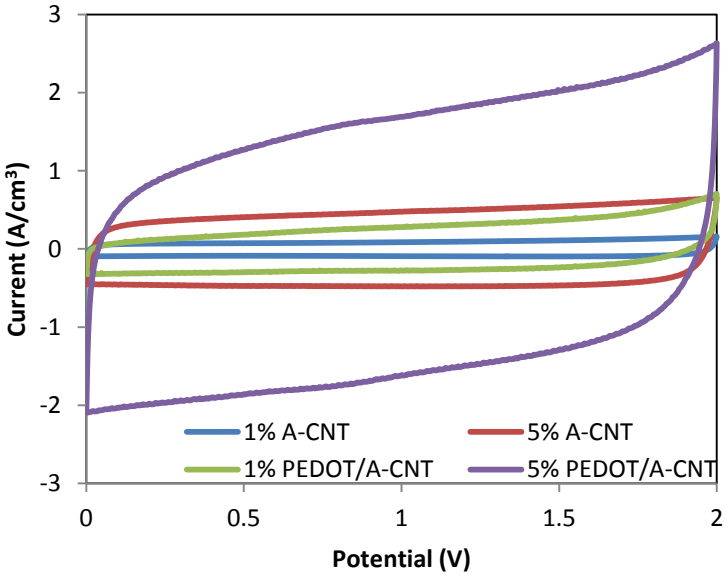

Figure 3.4: Volumetric CV curves of supercapacitor cells of each kind of electrode

The slow scan rate of CV curves allows supercapacitors to fully exhibit capacitance behaviors. Therefore, the capacitance values from slow scan rate CV will be slightly higher than high scan rate CV. For example, from Figure 3.5, the gravimetric specific capacitance of 5% PEDOT/A-CNT at scan rate 100 mV/s, 50 mV/s, and 20 mV/s are 201.37 F/g, 211.8 F/g and 221.68 F/g respectively.

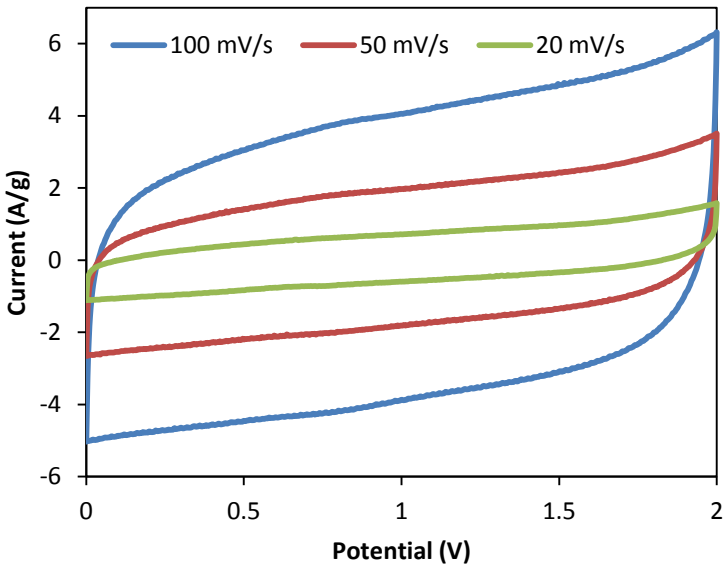

Figure 3.5 Gravimetric CV curves of 5% PEDOT/A-CNT with $EMIBF_4$/PC at different scan rates

3.2 Galvanostatic Charge-Discharge Tests: Electrodes

Galvanostatic curves demonstrate electrochemical behavior of each supercapacitor in each charge and discharge cycle. The small discharge rate will provide a longer discharge time which indicate more fully capacitance performance. As Figure 3.6, the discharge rate at 0.5 A/g have a longer discharge time than discharge rate at 10 A/g. When each type of electrode cells were compared at the same discharge rate as shown in Figure 3.7, the PEDOT/A-CNT cells provides a longer discharge time than uncoated samples indicating high capacitance storage.

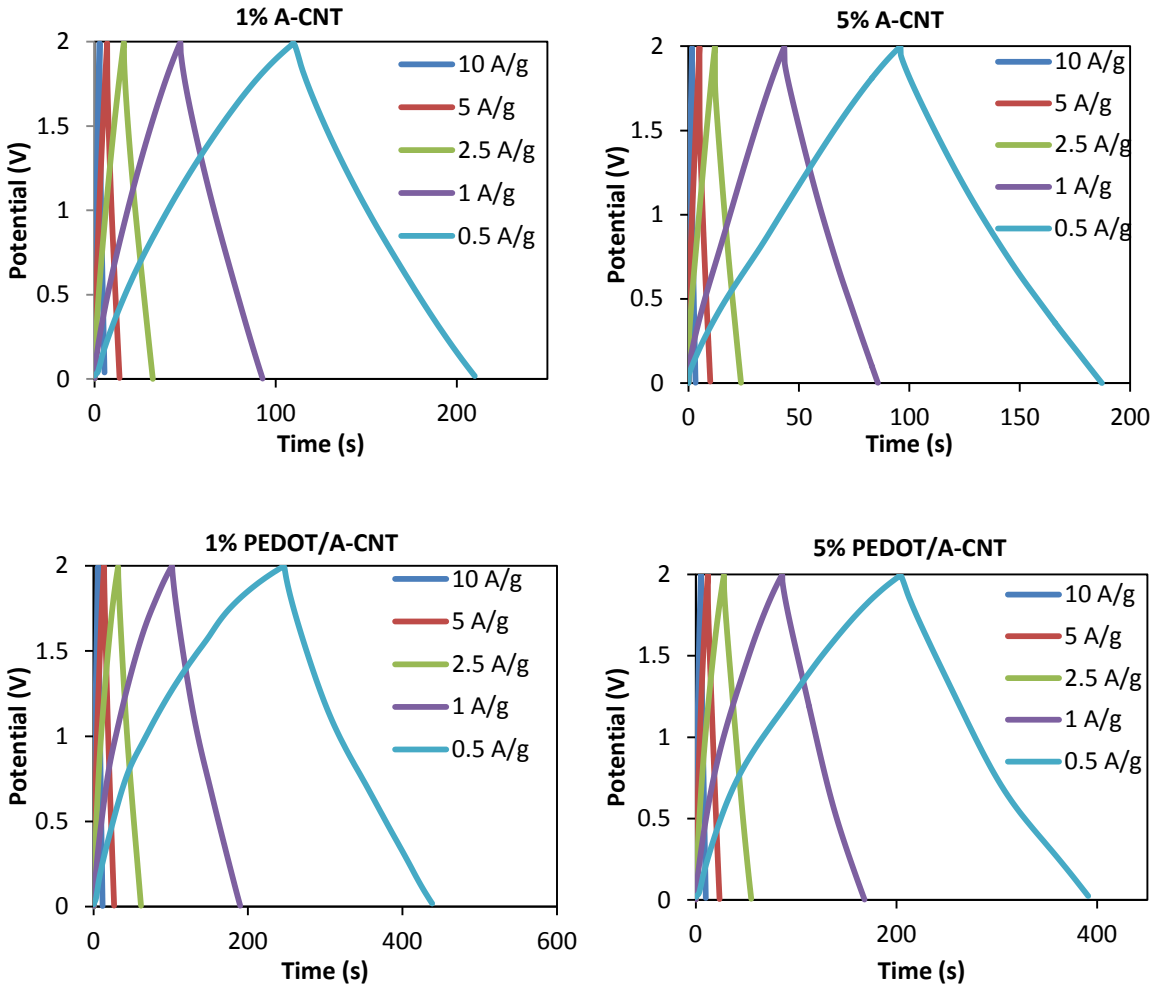

Figure 3.6: Galvanostic curves of supercapacitor cells of each kind of electrodes

To investigate the capacitance behaviors of each kind of electrodes, gravimetric and volumetric specific capacitance values at each discharge rate of each electrode sample were calculated from the slope after the IR voltage drop of the galvanostatic discharge curves as shown in Figure 3.8 and 3.9. For gravimetric comparison, the specific capacitance values at a discharge rate of 0.5 A/g of 1% A-CNT, 5% A-CNT, 1% PEDOT/A-CNT and 5% PEDOT/A-CNT are 106.4 F/g, 99.3 F/g, 220.6 F/g and 207.9 F/g respectively. For volumetric comparison, the specific capacitance values at a discharge rate of 0.5 A/g of 1% A-CNT, 5% A-CNT, 1%

PEDOT/A-CNT and 5% PEDOT/A-CNT are 3.9 F/cm^3, 18.6 F/cm^3, 13.8 F/cm^3 and 83.96 F/cm^3 respectively. Both gravimetric and volumetric capacitance values from galvanostatic tests also follow the same trend discussed from the CV curves. PEDOT coating considerably contributes more specific capacitance to the A-CNT electrodes. Also, the high volume fraction of A-CNT electrodes efficiently provides more capacitance per unit volume.

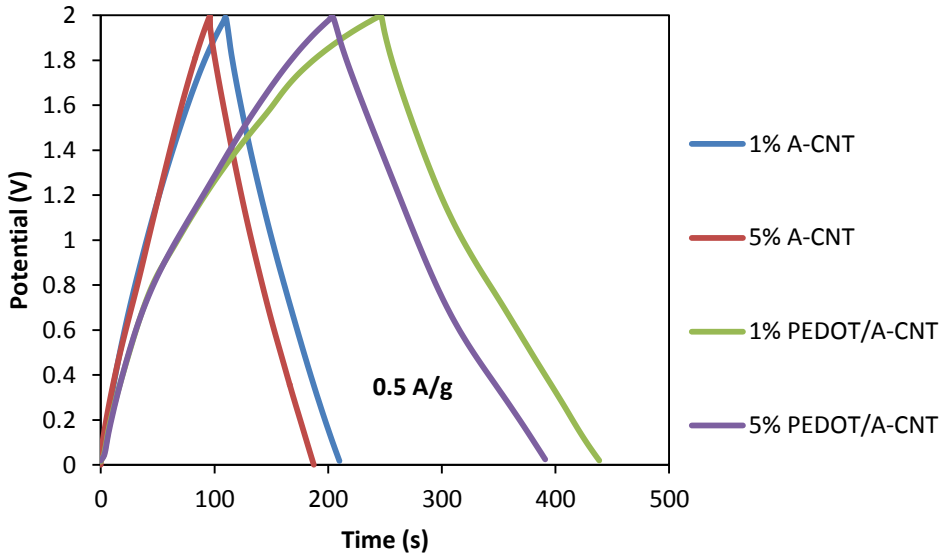

Figure 3.7: Galvanostic curves comparison at discharge rate 0.5 A/g

Gravimetric and volumetric energy density and power density also can be estimated from the galvanostatic test as shown in the Ragone plots of Figures 3.10 and 3.11. Due to the same operating voltage from 0-2 V for all samples, energy density proportions to capacitance value of the cell. The higher capacitance means generating higher energy density. The maximum gravimetric energy densities of 1% A-CNT, 5% A-CNT, 1% PEDOT/A-CNT and 5% PEDOT/A-CNT are 14.3 Wh/kg, 13.0 Wh/kg, 29.8 Wh/kg and 27.8 Wh/kg respectively. Also, the maximum volumetric energy densities of 1% A-CNT, 5% A-CNT, 1% PEDOT/A-CNT and 5% PEDOT/A-CNT are 0.5 Wh/L, 2.5 Wh/L, 1.9 Wh/L and 11.21 Wh/L respectively. These

energy density results totally follow similar trend as specific capacitance values. These results can be concluded that PEDOT coating and electrode densification method are the ways to improve the energy storage mechanism.

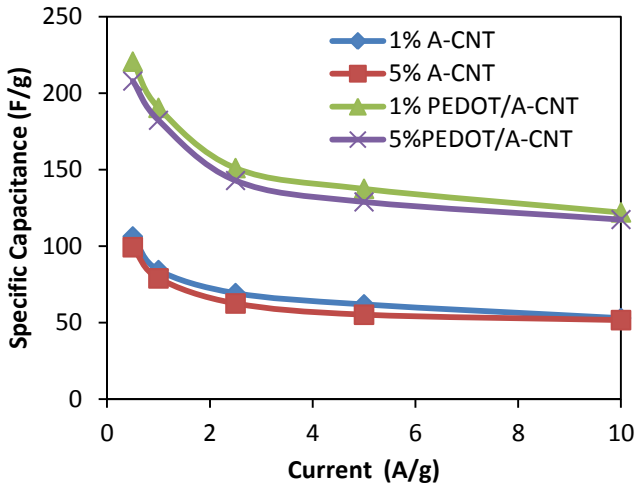

Figure 3.8: Gravimetric specific capacitance of each kind of electrodes from galvanostatic tests

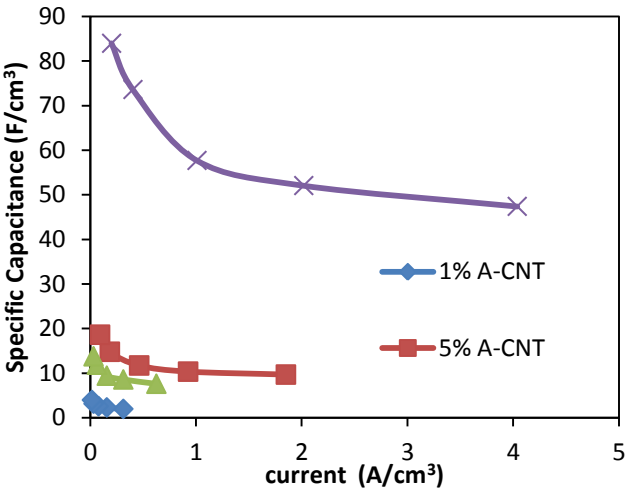

Figure 3.9: Volumetric specific capacitance of each kind of electrodes from galvanostatic tests

Power density related to kinetic activity of capacitive mechanism. The faster ions transport and conduction is the more power of supercapacitor can generate. Therefore, power

density is inversly proportional to the equivalent series resistance (ESR) of the cell. Then, ESR can be calculated from the IR drop or voltage loss when a current pass through a certain resistance. The more resistance and current is the more voltage drop following Ohm's law. The ESR values from IR drop is different from ESR in EIS test because ESR from IR drop is characterized in high voltage while ESR in EIS test is investigated at very low voltage (<0.05 V). However, ESR from both tests represent the same behavior of supercapacitors. IR drop can be observed at the beginning of each charge and discharge cycle. The plots of IR drop from each electrode sample were collected as shown in Figure 3.12. Comparison at similar current density, the IR drop values of 1% samples are lower than 5% samples because there are more empty spaces between nanotube as ion pathways in 1% samples for ions to diffuse easier and faster than in 5% samples [51,52,54]. Moreover, the polymer coated samples have smaller IR drops than uncoated samples. Because PEDOT is a conducting material, the coated electrodes become strong electronic attraction to ions which improve the electronic drifting of ion transports [19]. Therefore, IR drops lead the trend of gravimetric power density. The power density values of the same volume fraction samples are in the same range. The coated sample has slightly higher in power density. The 1% PEDOT/A-CNT has the highest power density about 125 kW/kg. However, when the charge-discharge rate becomes small which allow the capacitance mechanism to slowly proceed, the power density of all samples become less significantly different. At discharge rate 0.5 A/g, the gravimetric power densities are 26.9 kW/kg, 26.0 kW/kg, 34.7 kW/kg and 28.4 kW/kg for 1% A-CNT, 5% A-CNT, 1% PEDOT/A-CNT and 5% PEDOT/A-CNT respectively. For volumetric power density, the trend seems to follow the ratio of conductive materials to the surface area of the electrodes. In this study where all electrodes have the same thickness, the 5% PEDOT/A-CNT show the highest power density per unit

volume. At discharge rate 0.5 A/g, the gravimetric power density are 1.0 kW/L, 4.88 kW/L, 2.17 kW/L and 11.54 kW/L for 1% A-CNT, 5% A-CNT, 1% PEDOT/A-CNT and 5% PEDOT/A-CNT respectively

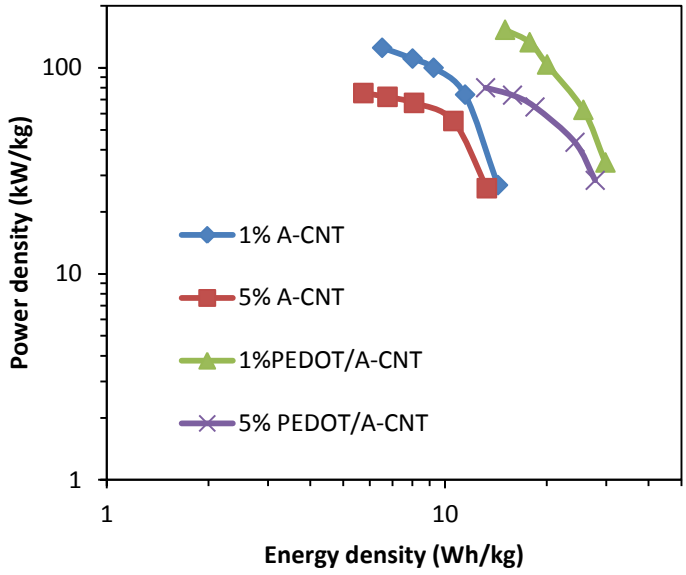

Figure 3.10: Gravimetric Ragone plot of supercapacitor cells of each kind of electrodes

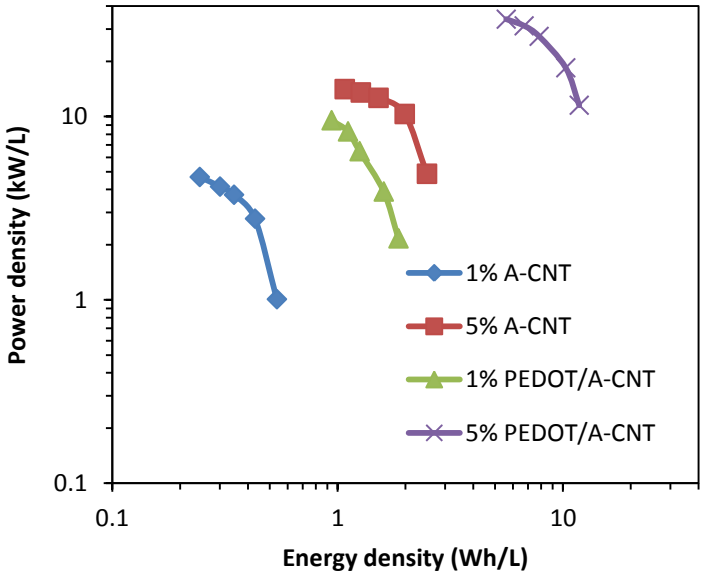

Figure 3.11: Volumetric Ragone plot of supercapacitor cells of each kind of electrodes

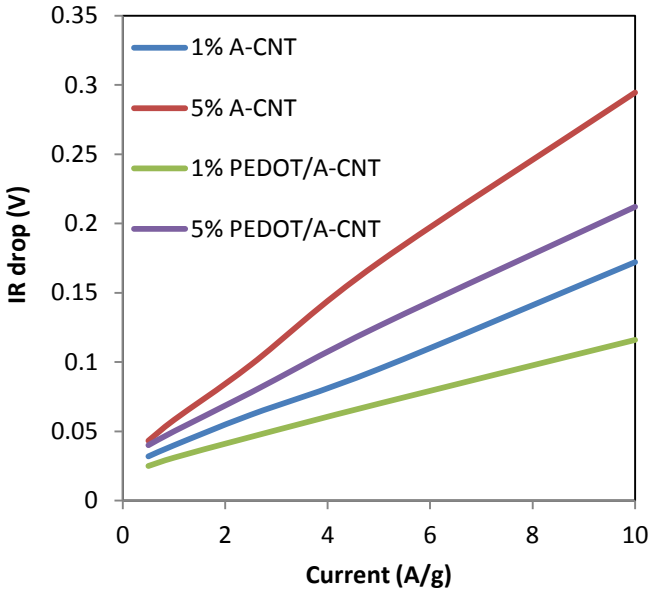

Figure 3.12: IR voltage drops of supercapacitor cells of each kind of electrodes

3.3 Electrochemical Impedance Spectroscopy (EIS): Electrodes

EIS measurements were investigated for each electrode sample cell in order to understand the ion diffusion and drifting process in the range of frequency 10 mHz to 1 MHz. The Nyquist plot of each sample is shown in Figure 3.14. The capacitive behaviors of each supercapacitor were observed as the steep increasing linear slope of imaginary impedance part at low frequency regions. Then, the ion transport behaviors to electrodes were observed as semicircle shape in the high and mid frequency regions [50]. From Figure 3.14, the Nyquist plot showed 2 semicircles in coated samples implying two diffusion layers. However, coating electrodes is not necessary to always show double semicircles. There are many factors such as electrolyte concentration, impurity and electrode contacts to affect the equivalent circuit. From the previous study [55], the simplified equivalent circuit of A-CNTs has been characterized as the Figure 3.13 where C_1 and R_1 are capacitance and resistance from interface of ionic liquid and gold current collectors. C_2 and R_2 are capacitance and resistance from interface of ionic liquid and electrodes. C_3 and R are

capacitance and resistance of the electrode with the electrolyte media. W is the Warburg element which is related to a diffusion parameter. The uniform PEDOT coating will especially increase capacitance in C_2 due to a pseudo-capacitive mechanism while the coating will reduce resistance in R_2 due to the conductive properties of the PEDOT. The true equivalent circuit of PEDOT/A-CNT will be more complicated than Figure 3.14 which can be studied in the future. Equivalent Series resistance (ESR) was determined to be 12.69 ohm for 1% A-CNT, 12.05 ohm for 5% A-CNT, 12.36 ohm for 1% PEDOT/A-CNT and 11.78 for 5% PEDOT/A-CNT. These ESR values are consistent with volumetric power density. Also, the highest volumetric capacitance as 5% PEDOT/A-CNT would have the lowest size of impedance plot as equation:

$$Z_C = 1/(j\omega C) \qquad (1)$$

Where C is the capacitance and ω is the angular frequency

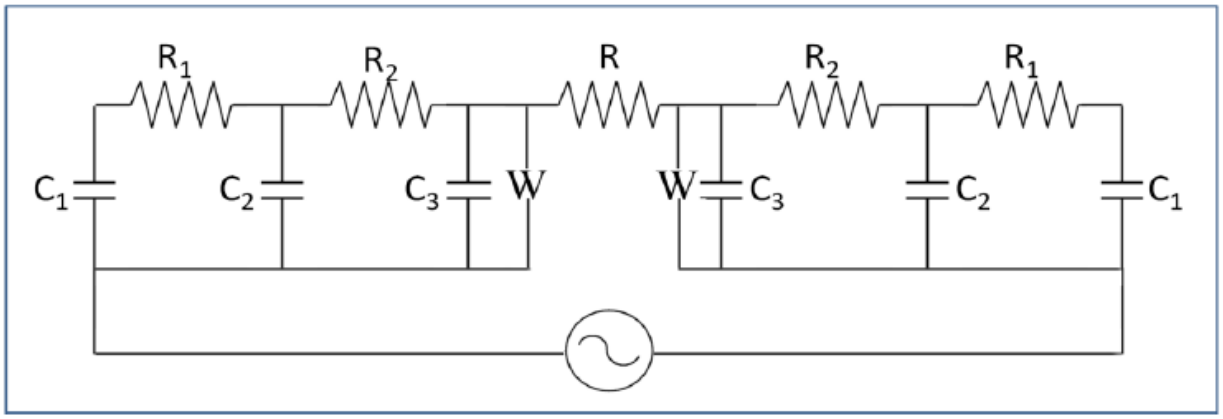

Figure 3.13: Equivalent circuit of A-CNT supercapacitor electrodes [55]

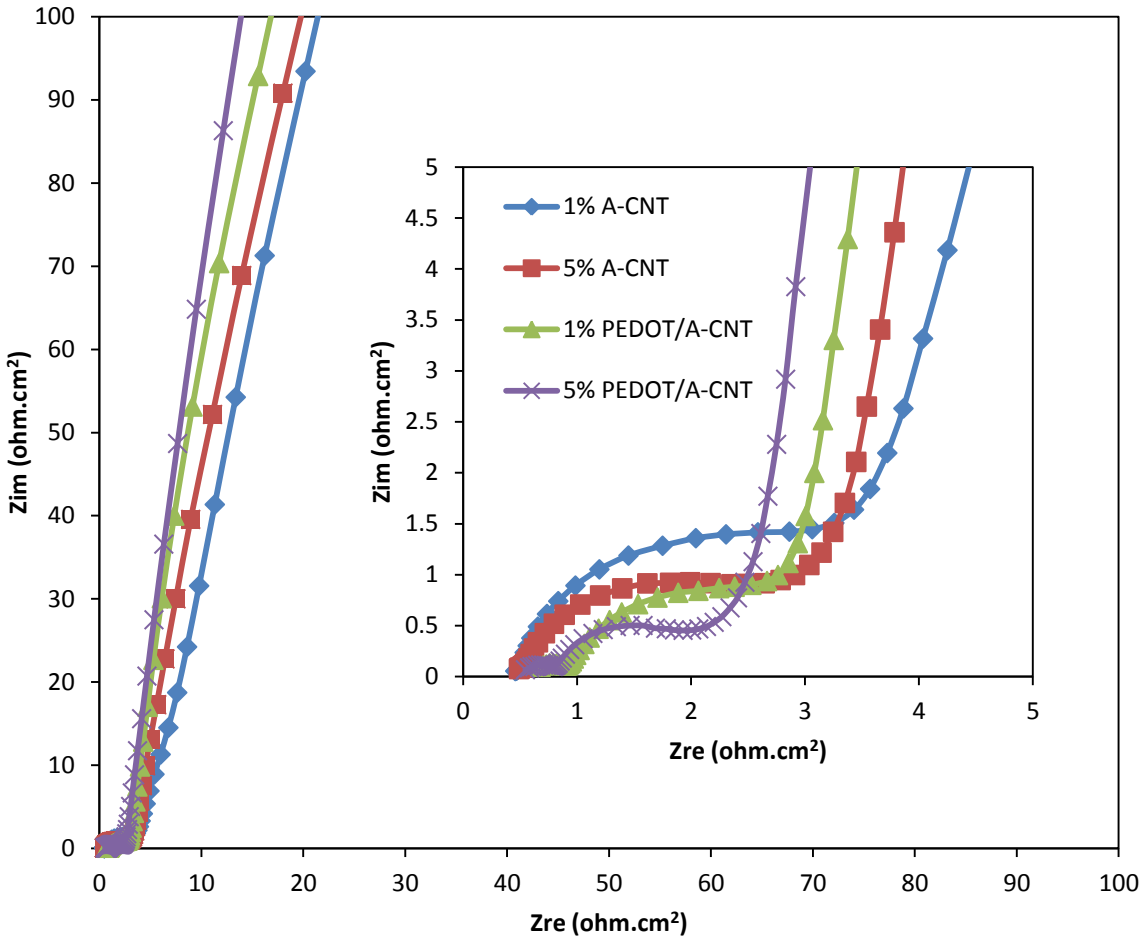

Figure 3.14: Nyquist plots of supercapacitor cells of each kind of electrodes

The real capacitance (C') of each sample calculated from EIS were plotted as a function of frequency to more deeply observed capacitive behavior on electrodes as shown in Figure 3.15. All samples behave in the same way that real capacitance values rapidly increase at the mid range of the frequency and then slowly decrease at further low frequency as electrodes starting to reach its full capacitance. These capacitive behaviors corresponding to frequency illustrate a double layer capacitive mechanism of ions with micropores in the electrodes [53]. Nevertheless, the real capacitance values of coated samples are much higher than uncoated samples due to the

support of pseudo-capacitance of conducting polymer. The trend of real capacitance is consistent with the gravimetric capacitance of both CV and galvanostatic tests.

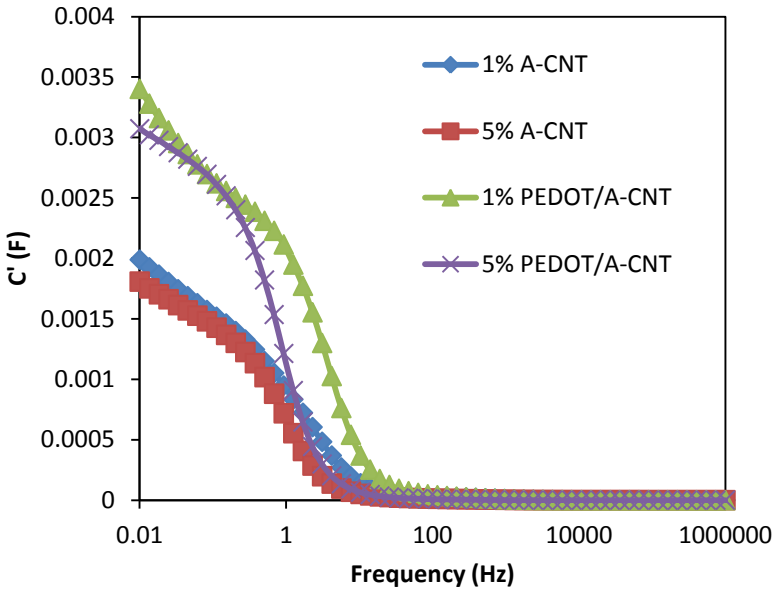

Figure 3.15: Real capacitance part from impedance of each electrode samples

The imaginary capacitance (C'') from EIS interprets how fast supercapacitors can store and discharge energy. As the plot of C'' vs frequency, the peak of the plot indicates knee frequency (f_k) which will be calculated to be characteristic time constant ($t = 1/f_k$) . The small value of the time constant demonstrates high speed of energy delivery [53]. From Figure 3.16, time constant of 1% A-CNT, 5% A-CNT, 1% PEDOT/A-CNT and 5% PEDOT/A-CNT are 0.59 s, 1.07 s, 0.32 s, and 0.88 s respectively. The trend of these time constant values is consistent with IR voltage drop and gravimetric power density in galvanostatic tests. The more ion pathways in aligned structure and conducting polymer facilitate fast ion mobility in electrochemical respond of applications.

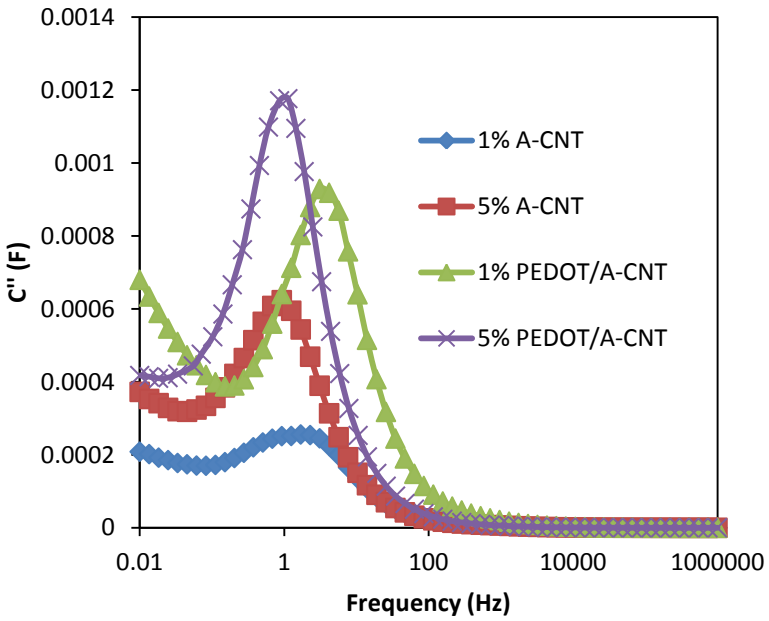

Figure 3.16: Imaginary capacitance part from impedance of each electrode samples

3.4 Capacitance Retention: Electrodes

Each symmetric supercapactitor cell for each electrode sample performed 1000 cycles of galvanostatic test and then determine the maintain capacitance as the stability of the devices (Figure 3.17). The result indicated that uncoated A-CNT has very stable performance (99.34% for 1% A-CNT and 98.81 for 5% A-CNT) while the performance of PEDOT samples are degraded about 10 % from initial capacitance (91.54% for 1% PEDOT/A-CNT and 89.92% for 5% PEDOT/A-CNT). The structure of PEDOT polymer can generate high strain and deform with repeated ion propagation cycles leading to electrode malfunction. Therefore the failing structure results in degraded capacitive behavior and a drop in overall device performance. However, from another study from our group, PEDOT coated on random orientation CNT electrodes are utilized to compare and observe the retention with PEDOT/A-CNT sample as shown in Figure 3.18 [46]. The study indicates that PEDOT/random-CNT lost high capacitance

more than PEDOT/A-CNT after 1000 cycles. The unorganized coating structure could easily break down and disrupt ion conduction and propagation on CNTs [14]. Therefore, aligned structure electrodes not only contribute high accessibility for ions but also allow conformally coated polymer to have longer life time function.

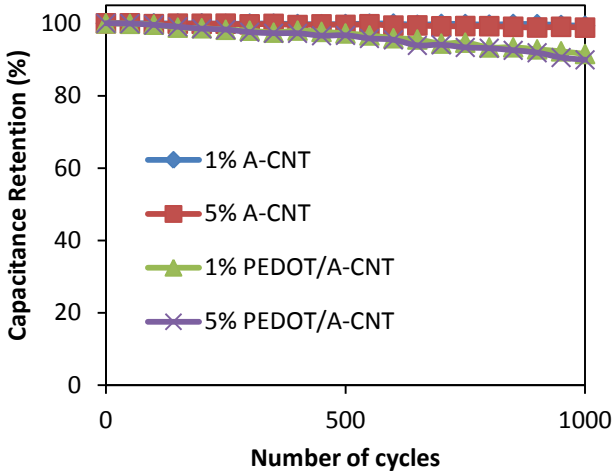

Figure 3.17: Capacitance retention of supercapacitor cells of each kind of electrodes

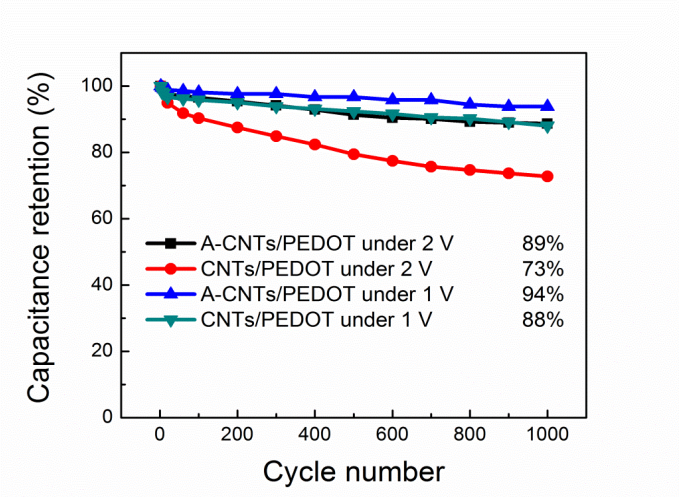

Figure 3.18: Capacitance retention of supercapacitor cells of PEDOT coated on A-CNT and random CNT with $BMIBF_4$/PC under 1 and 2 V [46]

3.5 Coulombic Efficiency: Electrodes

Coulombic efficiency (Eff) can be simply estimated from the capacitance slope of charge and discharge in one cycle of galvanostatic test. The coulombic efficiencies of each electrode sample are shown in Table 3.1. From Table 3.1, the non-coated A-CNT samples have higher efficiency than PEDOT/A-CNT samples because there are some losses or irreversible processes of charge ion propagation on the polymer coating. Also, the 1% volume fraction samples have lower efficiency than 5% volume fraction samples because 1% samples have more empty spaces and areas of current collector electrodes that allow causing more current leakage than 5% densified samples. The charge-potential or QV curves are introduced in this section to closely observe the charge storage behavior and the loss in one cycle. From the capacitance equation [6]:

$$Q = CV \quad (2) \quad , \quad Q = \int I dt \quad (3) \text{ and } \quad E = \frac{1}{2} QV \quad (4)$$

Where Q is the amount of charge, V is the operating voltage, C is the capacitance, I is the current and t is the charge-discharge time. When the currents of CV curves and galvanostatic curves are integrated with charge-discharge time, the QV curves will be represented. The area above charge and discharge curves to the maximum Q in QV plot is demonstrated the total energy that is actually stored and discharged in one cycle. The difference between charge-discharge areas or the loop means the energy loss from the charge storage process. The bigger of the charge-discharge loop is the more loss or the lower coulombic efficiency (Eff = 1 – loss). The difference of Q values at zero voltage shows the amount of current leakage as well. From the QV plots of each sample in Figure 3.19 and 3.20, Eff from both CV and galvanostatic curves show the same trends as previous calculation from charge-discharge capacitance. The non-coated A-CNT and high volume fraction samples have higher efficiency than PEDOT/A-CNT and low volume fraction samples. However, the QV curves from CV curves show much higher loss than

from galvanostatic curves. Because the scan rate of CV is very high (100 mV/s or 40 s/cycle or 0.025 Hz), the fast charge-discharge process will cause more current leakage. In galvanostatic test (0.5 A/g or 200-400 s/cycle or 0.0025-0.005 Hz), the charge-discharge process is occurred at very low frequency, the slow stable mechanism provides higher Eff. The coulombic efficiency from QV in Figure 3.19 and 3.20 are listed in Table 3.1 as well.

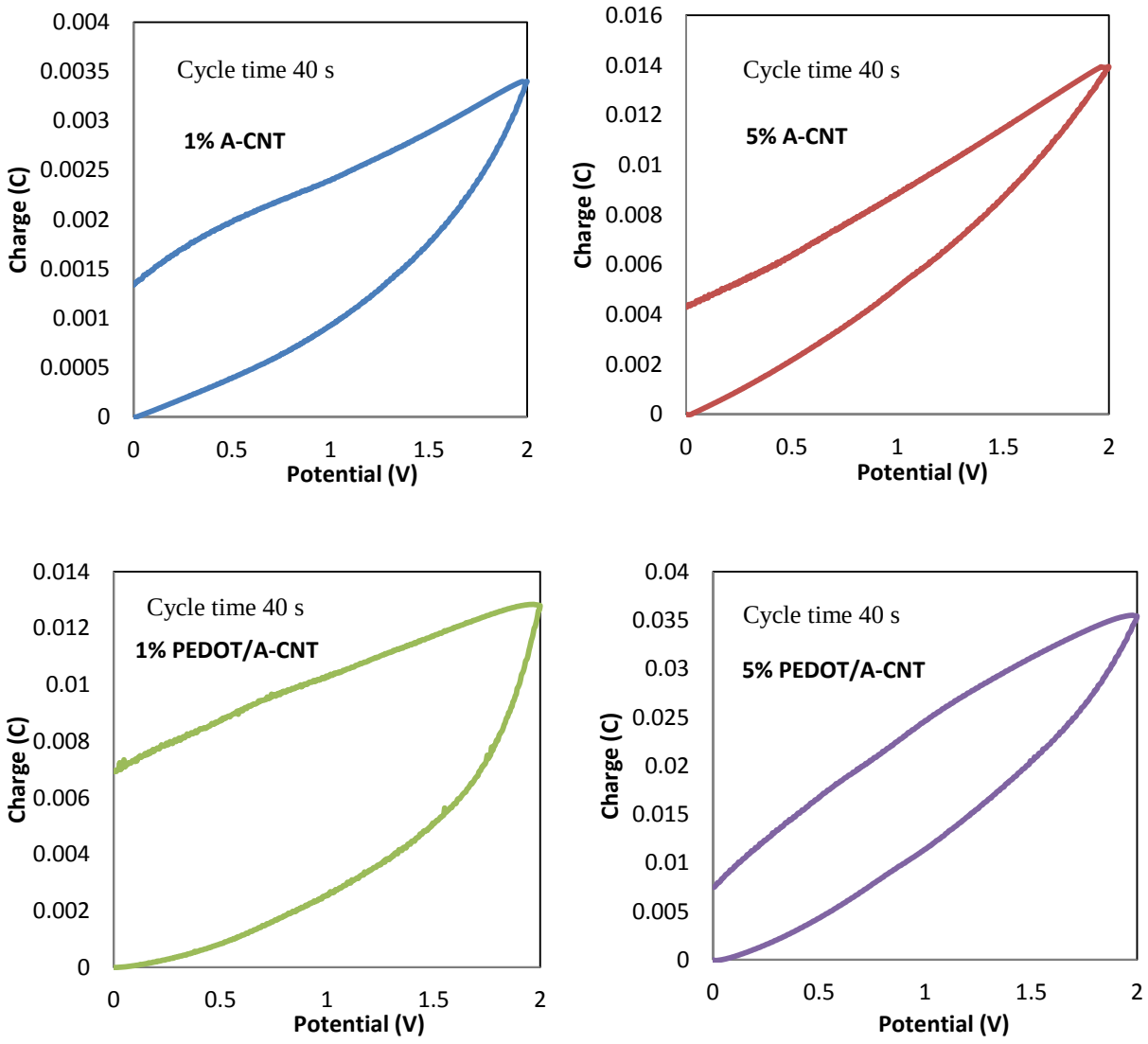

Figure 3.19: QV curves of each electrode sample from CV at scan rate 100 mV/s

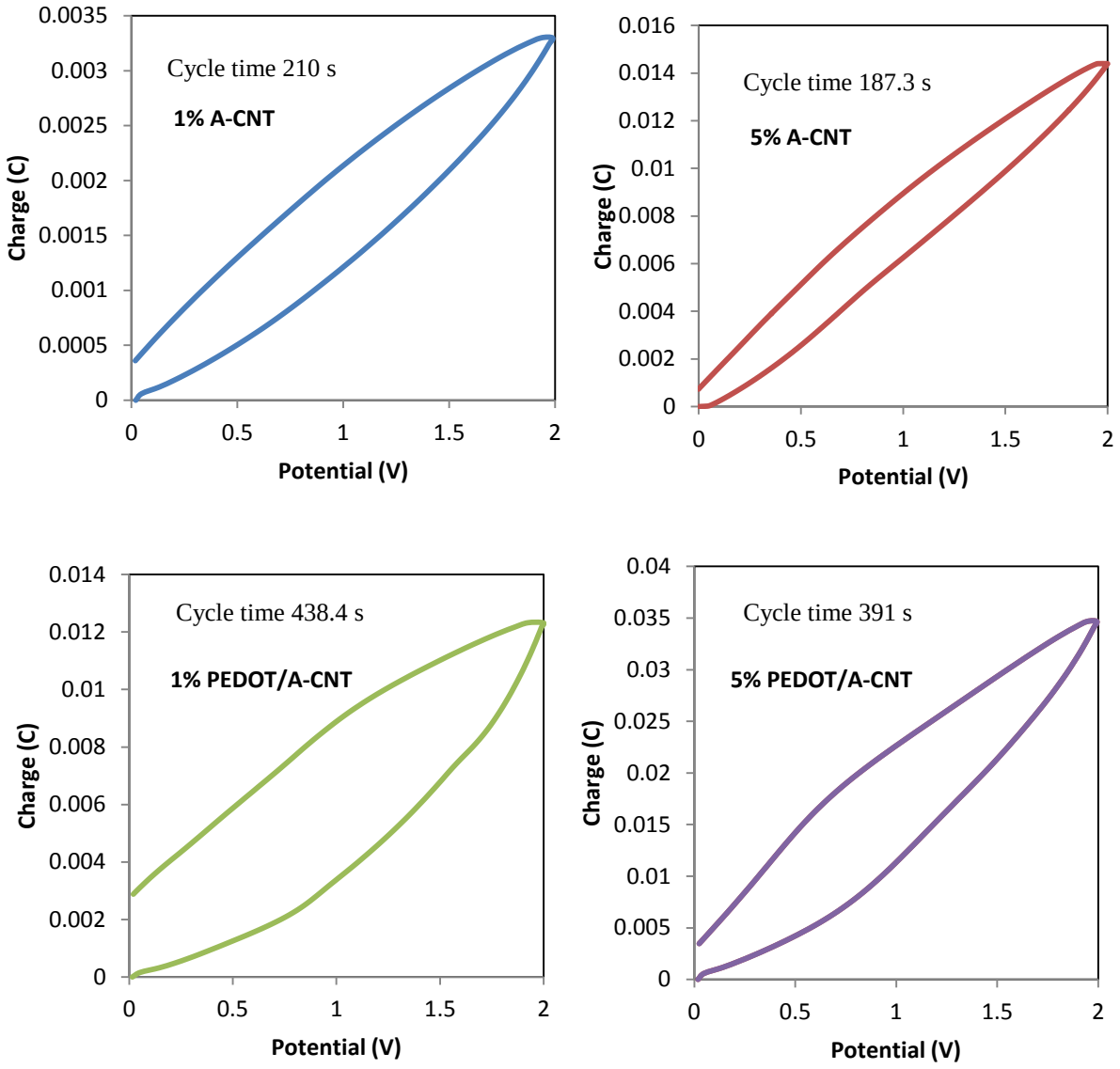

Figure 3.20: QV curves of each electrode sample from galvanostatic test at charge-discharge rate 0.5 A/g

Electrode	% Efficiency (from Capacitance at 0.5 A/g)	% Efficiency (from Figure 3.19)	% Efficiency (from Figure 3.20)
1% A-CNT	92.59	61.59	82.18
5% A-CNT	93.22	75.83	88.56
1% PEDDT/A-CNT	87.37	37.44	70.46
5% PEDOT/A-CNT	91.26	71.62	78.85

Table 3.1: Coulombic Efficiency of each electrode sample

Another way to determine the coulombic efficiency is to estimate the loss from the ratio of imaginary and real part capacitance in EIS. From Figure 3.21, it shows that the loss is depended on frequency. The loss will increase drastically when approach high field or high frequency. The high volume fraction A-CNT and coated samples will have more loss energy at high frequency than low volume fraction A-CNT and non-coated samples. However, at low field or low frequency, the loss behavior of supercapacitor will act differently depending on many factors such as relaxation effect and types of electrolyte. In this supercapacitor application, the capacitive behaviors usually occur at very low frequency which some are beyond limit of experiment. The results and trends will be more conclusive when more low frequency measurement is precisely conducted.

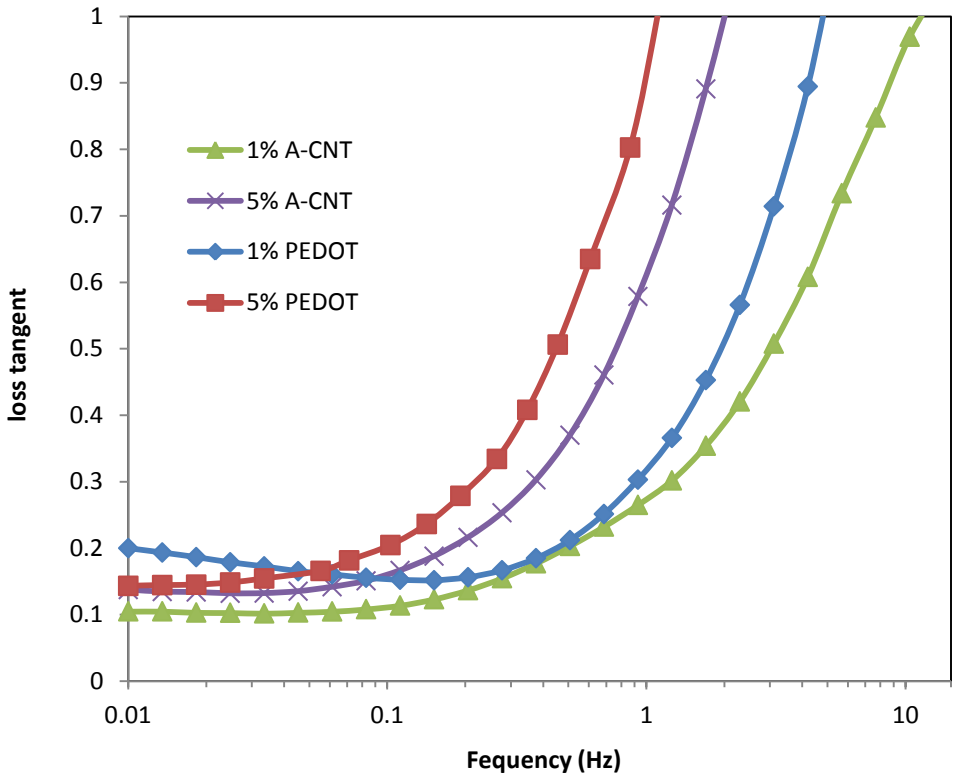

Figure 3.21: Loss vs frequency from C'' and C' in EIS of each electrode sample

Chapter 4

Results and Discussion: Electrolytes

In this chapter, two new ionic liquids: $Pyr_{14}TFSI$ (N-Butyl-N-methylpyrrolidinium bis(trifluoromethanesulfonyl) imide) and EMITFSI (1-ethyl-3-methylimidazolium bis(trifluoromethanesulfonyl) imide) are introduced the further study about electrolyte effects on the best symmetric supercapacitor cell in chapter 3 which is 5% volume fraction PEDOT coated on aligned carbon nanotube (5% PEDOT/A-CNT) electrodes. The same characterizations on cyclic voltammograms, galvanostatic charge-discharge test, electrochemical impedance spectroscopy, and capacitance retention in chapter 3 are applied. However, this time, each sample cell has the same symmetric 5% PEDOT/A-CNT electrodes with different electrolytes: three pure ionic liquids $EMIBF_4$, EMITFSI, $Pyr_{14}TFSI$ and mixtures (1 M of EMITFSI/PC and 1M of $Pyr_{14}TFSI$/PC) for comparison. The effects of different anions ($TFSI^-$ andBF_4^-) and cations (EMI^+ and Pyr_{14}^+) and the effects of solvent PC on energy storage performance are expected to be observed.

4.1 Electrochemical Window (EW) and Cyclic Voltammograms (CV): Electrolytes

Electrochemical window is again the first property to be characterized to determine favorable operating voltages especially when new electrolytes were introduced to the system. From chapter 1, the electrochemical widow of EMITFSI and $Pyr_{14}TFSI$ are 4.6 and 5.9 V that both are higher than $EMIBF_4$ (4.5 V). The higher electrochemical widows of these ionic liquids are expected to help extend operating voltage. Therefore, the electrochemical window of 5% PEDOT/A-CNT symmetric cell with EMITFSI and $Pyr_{14}TFSI$ were determined with CV curves

from 0 to 3.5 V as shown in Figure 4.1 and Figure 4.2. The CV curves of EMITFSI and $Pyr_{14}TFSI$ are both stable from 0 up to 2.2-2.4 V (Black lines) then bumps and peaks indicated reactions start to appear. Compared with electrochemical window of $EMIBF_4$ with PEDOT/A-CNT in chapter 3 (0-2.2 V), the results from new ionic liquids are only slightly different. This is because the limiting potential comes from conducting polymer PEDOT that cannot tolerate high voltages as discussed in chapter 3, the operating voltage of the cell cannot be further extended. Consequently, the cells were selected to operate at 2 V as chapter 3 as well.

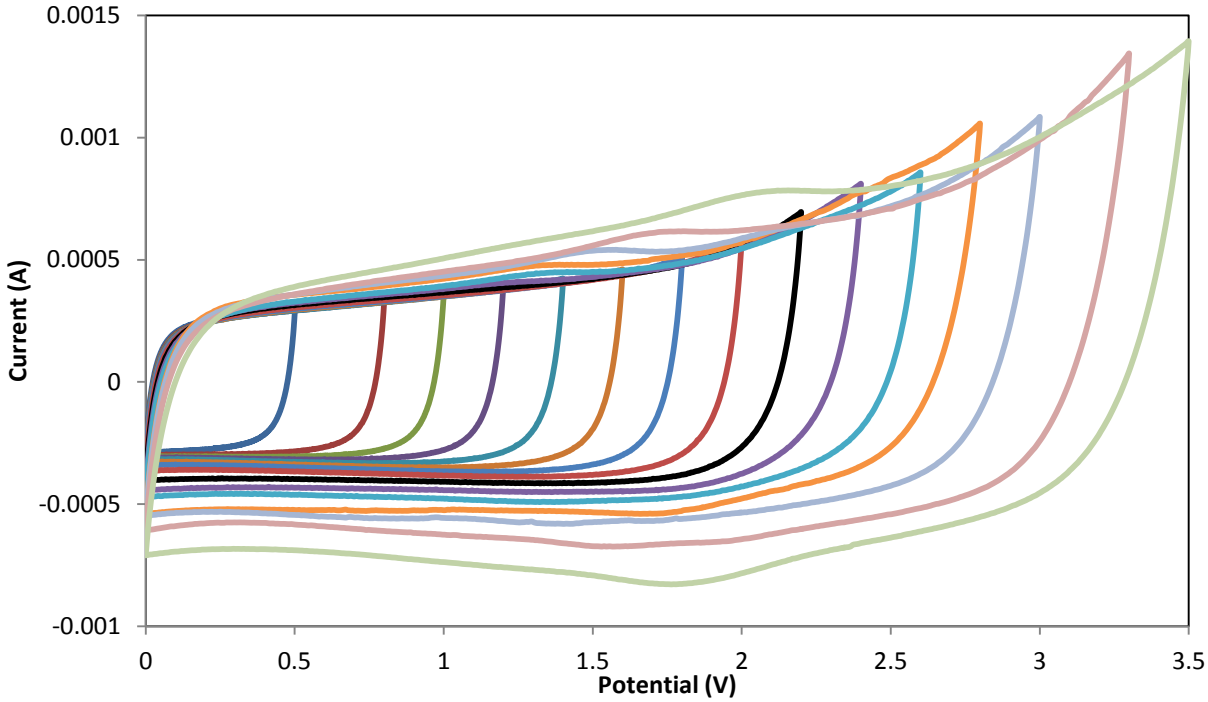

Figure 4.1: CV curves of PEDOT/ACNT with EMITFSI illustrated electrochemical widow of the cell

The CV curves of three ionic liquid: $EMIBF_4$, EMITFSI and $Pyr_{14}TFSI$ in 5% PEDOT/ ACNT symmetric supercapacitor cells are evaluated as shown in Figure 4.3. Because this time there is no difference in electrodes in comparison, the gravimetric graph is enough to represent capacitance performance with different electrolytes. The CV curves of all samples in Figure 4.3

are pretty stable in rectangular shapes at scan rate 100 mV from 0-2 V. Then, the specific capacitances from CV curves are estimated: 200.5 F/g for $EMIBF_4$, 180.6 F/g for EMITFSI, and 152.1 F/g for $Pyr_{14}TFSI$. $EMIBF_4$ electrolyte still shows the highest capacitance compared with those two new electrolytes. The reason behind this result is believed to come from the ion size of ionic liquids. From literature [56-57], the size of each ion has been investigated: [EMI^+] is 0.76 nm, [Pyr_{14}^+] is 1.10 nm, [BF_4^-] is 0.48 nm, and [$TFSI^-$] is 0.79 nm. Due to the fact that nanotube especially aligned structure is an open structure that allow ions to easily access and propagate on the surface area[58], the problem that large ions cannot access to micropores occurred in activated carbon[59] for capacitance are normalized. However, another problem become dominant that capacitance will depend on amount of ion penetrate and propagate on the surface area of electrodes. The small ions can arrange on the surface better than large ions. Then, $EMIBF_4$, which have both smallest anions and cations, can store more capacitance than the other two ionic liquids.

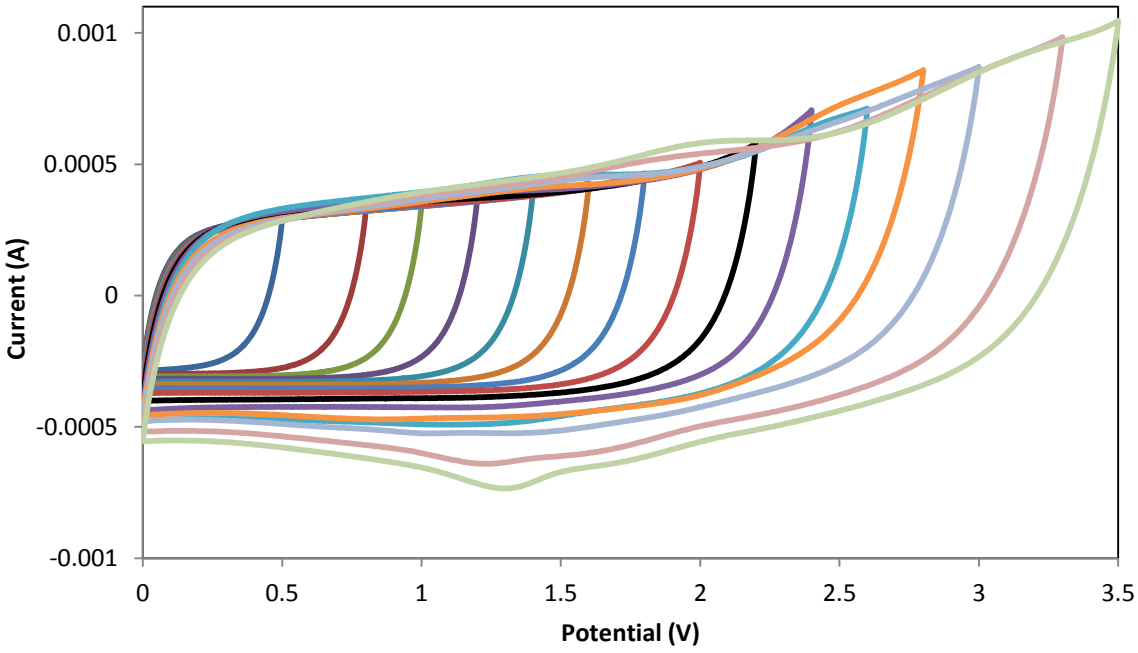

Figure 4.2: CV curves of PEDOT/ACNT with $Pyr_{14}TFSI$ illustrated electrochemical widow of the cell

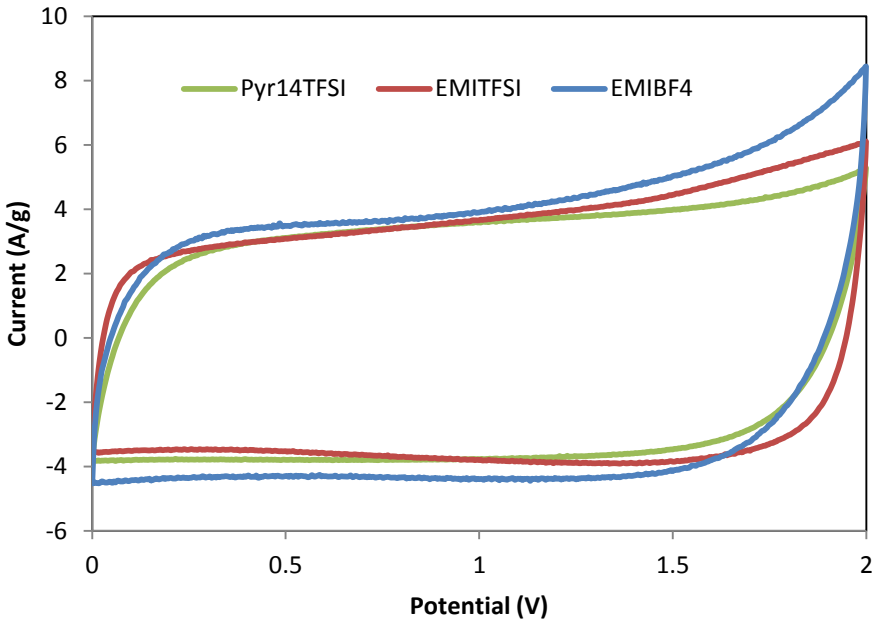

Figure 4.3: CV curves of three different pure ionic liquid supercapacitor cells

The CV curves of EMITFSI/PC and Pyr_{14}TFSI/PC samples do not show significantly change on electrochemical window and capacitance compared with pure ionic liquid samples. PC also has wide electrochemical window (4.5 V from chapter 1) comparable and compatible with ionic liquids. The CV curves of mixture electrolytes still show stable rectangular shapes. Moreover, as mention in previous paragraph that electrodes already have opened structure to store ions at the surface, PC solvent has very small effect for ion propagation on this type of electrodes. Therefore, capacitance contribution from PC addition is not really significant as well. From Figure 4.4 and 4.5, specific capacitance of 5% PEDOT/A-CNT at scan rate 100 mV with 1M EMITFSI/PC is 182.3 F/g and with 1M Pyr_{14}TFSI/PC is 156.4 F/g. Nevertheless, the role of PC is much more involved with conductivity, mobility, and dissociation of ionic liquid ions. These effects will be presented and discussed later in this chapter.

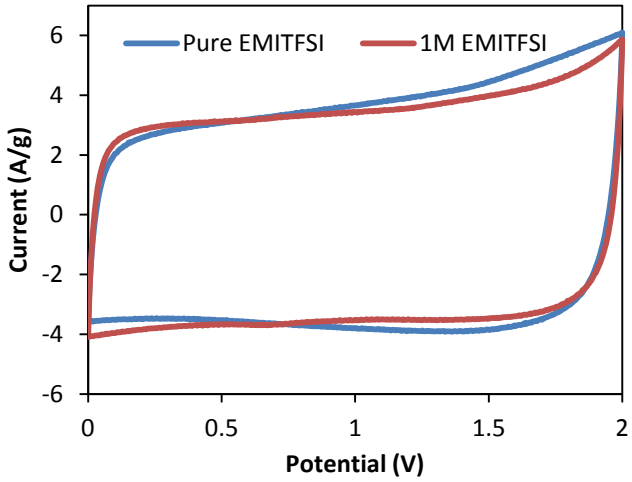

Figure 4.4: curves of 5% PEDOT/A-CNT with and without PC in the EMITFSI electrolyte

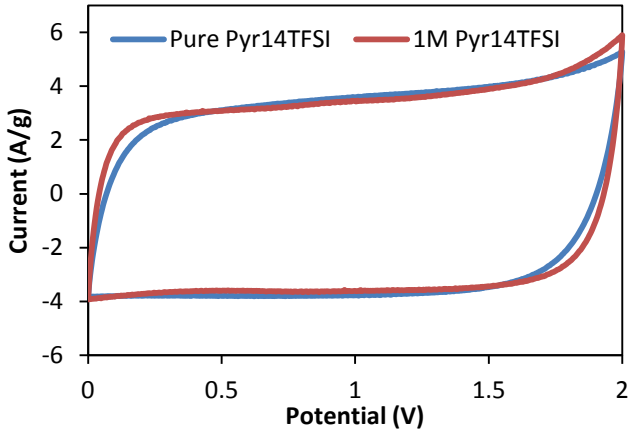

Figure 4.5: curves of 5% PEDOT/A-CNT with and without PC in the $Pyr_{14}TFSI$ electrolyte

4.2 Galvanostatic Charge-Discharge Tests: Electrolytes

Galvanostatic tests of each ionic liquid in 5% PEDOT/A-CNT symmetric cells at operating voltage 0-2 V are shown as Figure 4.6. The charge-discharge time indicated capacitance values of each kind of ionic liquid are different. Then, the slopes of those galvanostatic discharge curves are conversed to specific capacitance values as shown in Figure 4.7. At discharge current rate 0.5 A/g, the gravimetric specific capacitance values are 205.3 F/g, 184.9 F/g and 159.6 F/g for $EMIBF_4$, EMITFSI, and $Pyr_{14}TFSI$ respectively. These specific

capacitance values from Galvanostatic tests are consistent with the values from CV curves. $EMIBF_4$ shows the highest capacitance values to the high propagation of small size ions on electrode surfaces as discussed in previous section. Even though the volumetric graphs, which would have the same trend as gravimetric capacitance due to the same volumes of active electrode materials, are not shown in this thesis, for the record, the volumetric specific capacitance are estimated: 43.2 F/cm^3 for $EMIBF_4$, 38.9 F/cm^3 for EMITFSI and 33.6 F/cm^3 for $Pyr_{14}TFSI$.

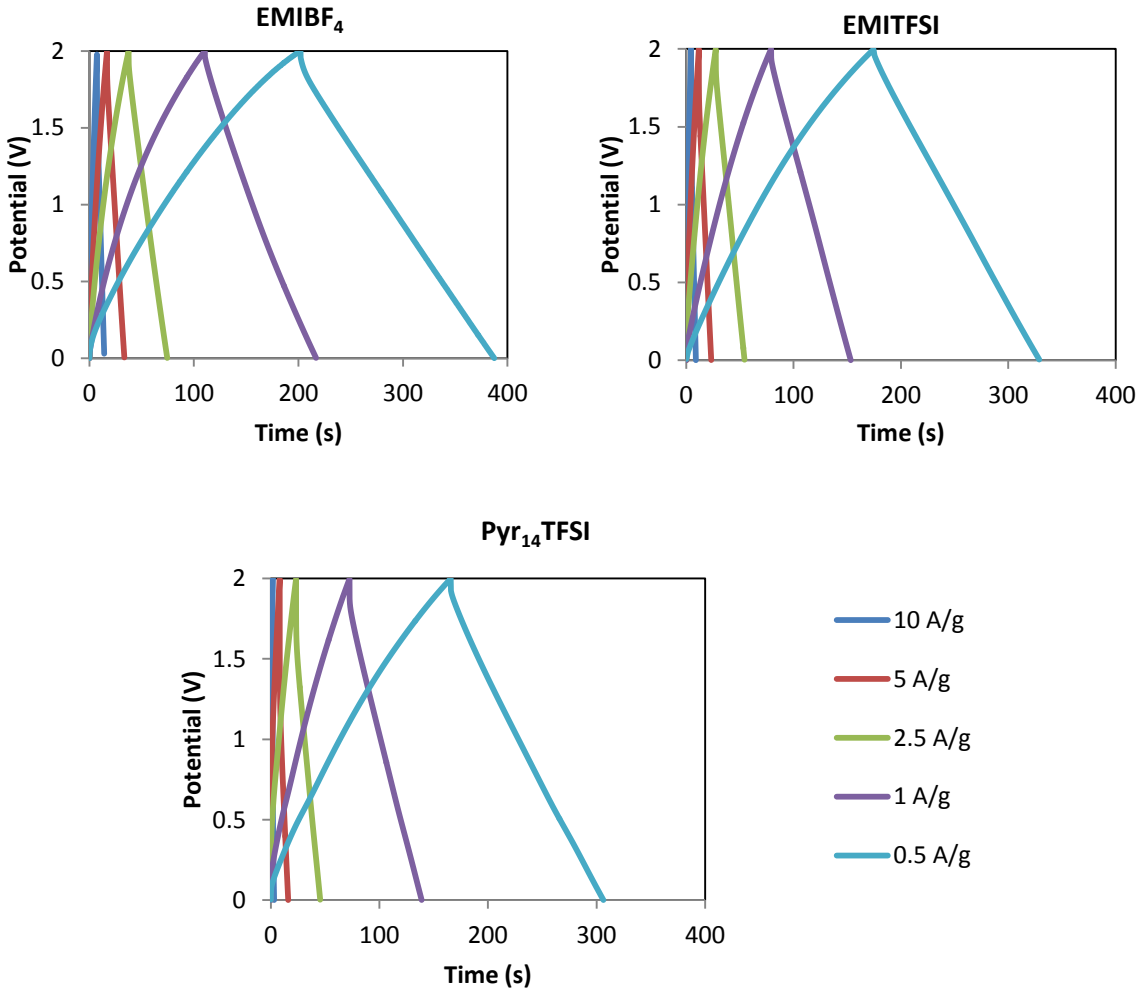

Figure 4.6: Galvanostatic curves of 5% PEDOT/A-CNT with three different pure ionic liquids

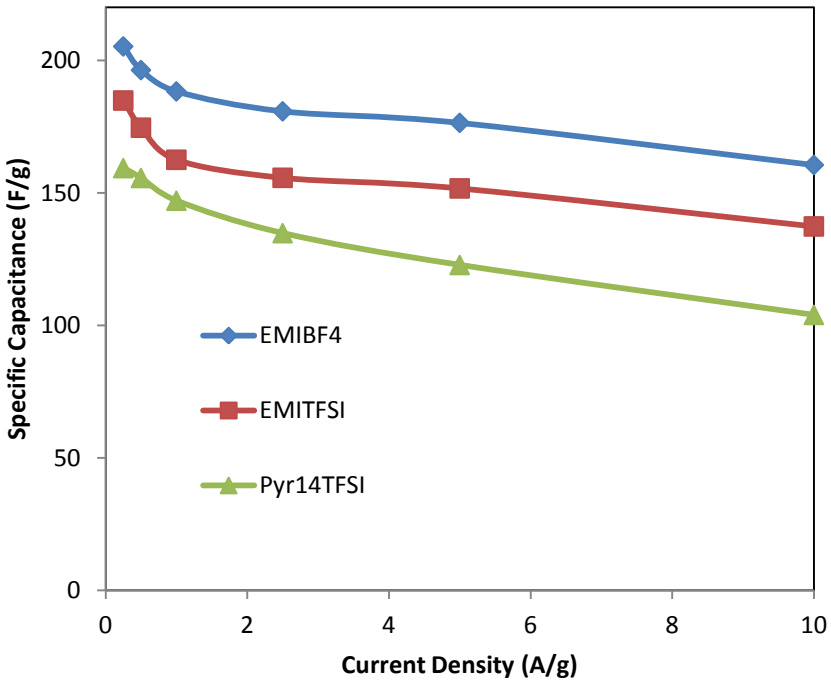

Figure 4.7: Gravimetric specific capacitance from galvanostatic tests of three pure ionic liquid samples

Galvanostatic test data were also analyzed for energy density and power density of each sample. Energy density is calculated from specific capacitance and operating voltage. Then, at the same voltage range from 0-2 V, the energy densities of each ionic liquid samples simply follow the trend of specific capacitance value as shown in Figure 4.8. These Ragone plot results demonstrate that ion size of ion liquids also have the similar effect on energy density as specific capacitance values discussed early. The $EMIBF_4$, which contains the highest capacitance, generate the highest energy density. The maximum energy densities at discharge rate 0.5 A/g are 28.0 Wh/kg for $EMIBF_4$, 24.9 Wh/kg for EMITFSI and 21.1 Wh/kg for $Pyr_{14}TFSI$. Also, for comparison, maximum volumetric energy densities are estimated: 11.6 Wh/L for $EMIBF_4$, 10.6 Wh/L for EMITFSI and 8.9 Wh/L for $Pyr_{14}TFSI$.

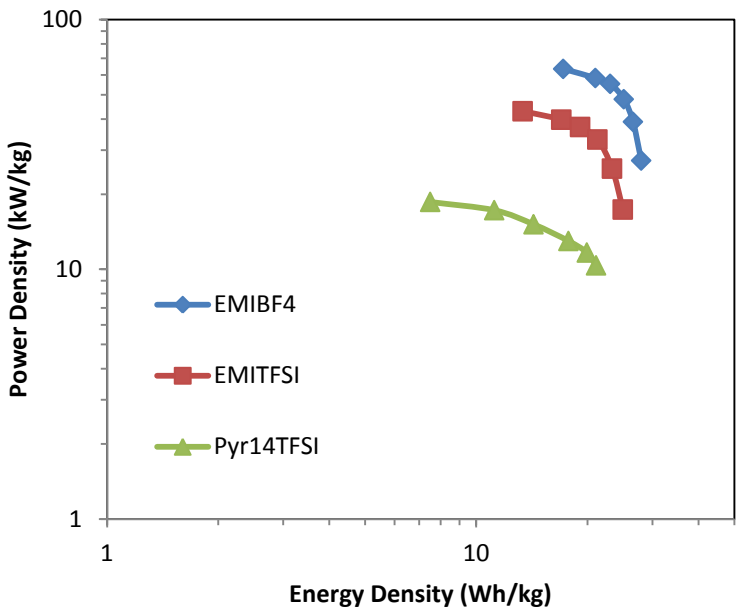

Figure 4.8: Gravimetric Ragone plots of three pure ionic liquid samples

Electrolytes also play an important role on power density. Because power density represents the rate of energy to be stored in or released from the devices, some kinetic properties of electrolytes such as conductivity, viscosity, and ion dissociation could be involved. The conductivity effect of electrolytes is illustrated as IR voltage drop in Figure 4.9. IR drop is inversely proportional to conductivity. $Pyr_{14}TFSI$ data shows a great amount of voltage drop meaning that this electrolyte has low ionic conductivity. These IR drop results are consistent with ionic liquid conductivity from the literature [32,36]. From ionic liquid properties table in chapter 1, $Pyr_{14}TFSI$ has the lowest conductivity (2.5 S/m) compared with EMITFSI (9.3 S/m) and $EMIBF_4$ (13.6 S/m). Moreover, the viscosity of $Pyr_{14}TFSI$ is very high (100 mPa.s) and ion size is large compared with the other ionic liquid, then ion diffusion will become slow for capacitive behaviors. From all these reasons, $EMIBF_4$ still generate the highest power density (63.5 kW/kg or 13.3 kW/L at discharge current 10 A/g) followed with EMITFSI (43.0 kW/kg or

9.1 kW/L) and $Pyr_{14}TFSI$ (18.6 kW/kg or 3.9 kW/L). In order to improve ionic liquids that suffer from low conductivity and high viscosity, a molecular organic solvent like PC in this case was mixed to the electrolytes. Molecular solvents provide many benefits such as more ion dissociation, high ion mobility and ion interaction with electrodes [45]. Nonetheless, this study only gives primary explanation for the results with PC solvent. More profoundly and fundamentally understanding of solvent effects would be focused in the future study. The concentration of 1 M of both EMITFSI/PC and $Pyr_{14}TFSI$/PC was selected for study and comparison due to the fact that, at this concentration, both mixtures show the highest power densities and provide enough ions to perform capacitive behaviors. Ragone plots of mixture samples are provided as shown in Figure 4.10 and 4.11. Power densities of both mixtures are much improved while there is no significant change in energy densities compared with the pure ionic liquid samples. For EMITFSI/PC, the maximum power density at discharge current 10 A/g is 68.8 kW/kg or 25.8 kW/L. For $Pyr_{14}TFSI$, the maximum power density is 53.3 kW/kg or 21.3 kW/L. These improvements of power density come from the reduction of ESR after mixing with PC solvent. The ESR information will be discussed again in the next section.

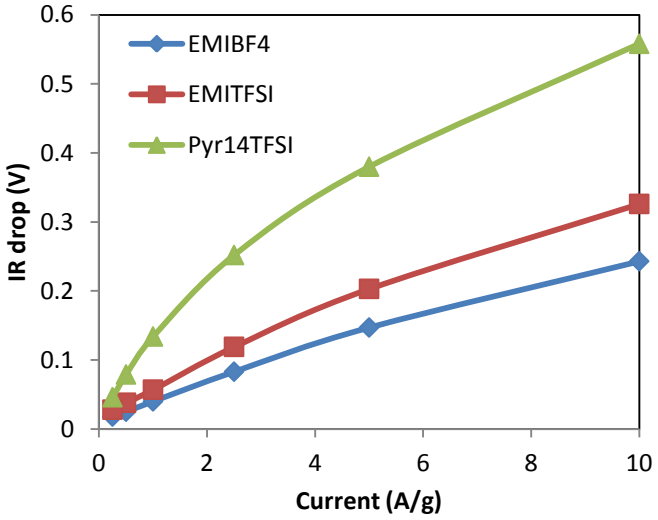

Figure 4.9: IR drop comparison between three different ionic liquids

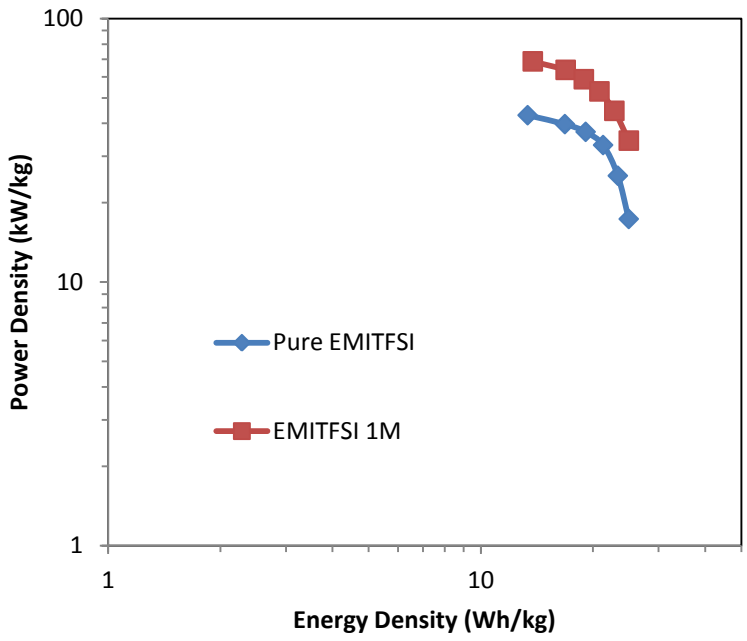

Figure 4.10: Ragone plot of EMITFSI with and without PC solvent

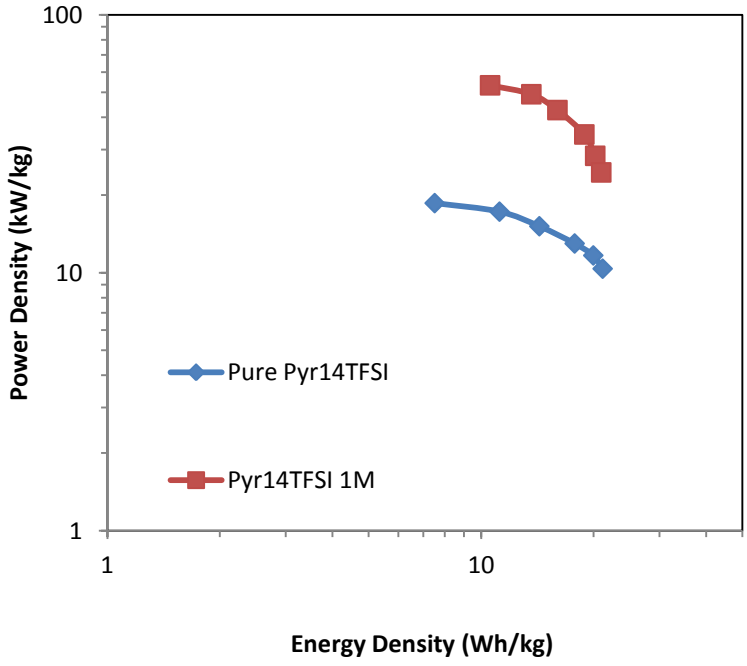

Figure 4.11: Ragone plot of $Pyr_{14}TFSI$ with and without PC solvent

4.3 Electrochemical Impedance Spectroscopy (EIS): Electrolytes

Nyquist plots for each ionic liquid sample from 10 mHz to 1 MHz were observed to analyze electrochemical behaviors with electrolyte effects as shown in Figure 4.12. EMITFSI and $Pyr_{14}TFSI$ cells illustrated excellent capacitive behaviors with the very steep slope at the low frequency region. But $EMIBF_4$ shows a slightly different capacitive behavior with a lower slope at very low frequencies. There are many factors that might affect $EMIBF_4$ to behave as this result such as electrodes-electrolyte contacts, impurity and current collectors. The way to diagnose the real reasons on this result is to figure out the equivalent circuit of the cells that is beyond the scope of this study. Nonetheless, the mid and high frequency regions of $EMIBF_4$ still show reasonable result as supercapacitors. The ESR values of each ionic liquid sample were determined: 12.9 Ohms, 16.98 Ohms, and 23.77 Ohms for $EMIBF_4$, EMITFSI and $Pyr_{14}TFSI$ respectively. These ESR values are coherent with the conductivity values gathered in the chapter 1 from literatures. $Pyr_{14}TFSI$ electrolyte has the highest resistance or lowest conductivity among ionic liquid samples leading to high voltage drop across the cell and low power density [60]. Then, PC molecular solvent which has low viscosity (2.8 mPa.s) was blended into electrolyte to enhance ion mobility of ionic liquids. As the Nyquist plot results showed in Figure 4.13 and Figure 4.14, ESR values of both EMITFSI/PC and $Pyr_{14}TFSI$/PC mixtures are reduced from the pure ionic liquid samples, especially $Pyr_{14}TFSI$. EMITFSI which already had fairly high ion mobility was slightly improved in ESR values to 12.84 Ohms from PC solvent effect while $Pyr_{14}TFSI$ which suffered from slow ion mobility became greatly reduced to 13.98 Ohms in ESR values with PC. These solvent effects were observed in higher power density in the previous section. However, this result is quite the limit that PC can help in ion migration. Lower concentration might have lower conductivity but the capacitance performance will start to suffer.

In order to improve more mobility issue, other molecular liquids with higher mobility properties such as acetonitrile (AN) should be introduced for future study.

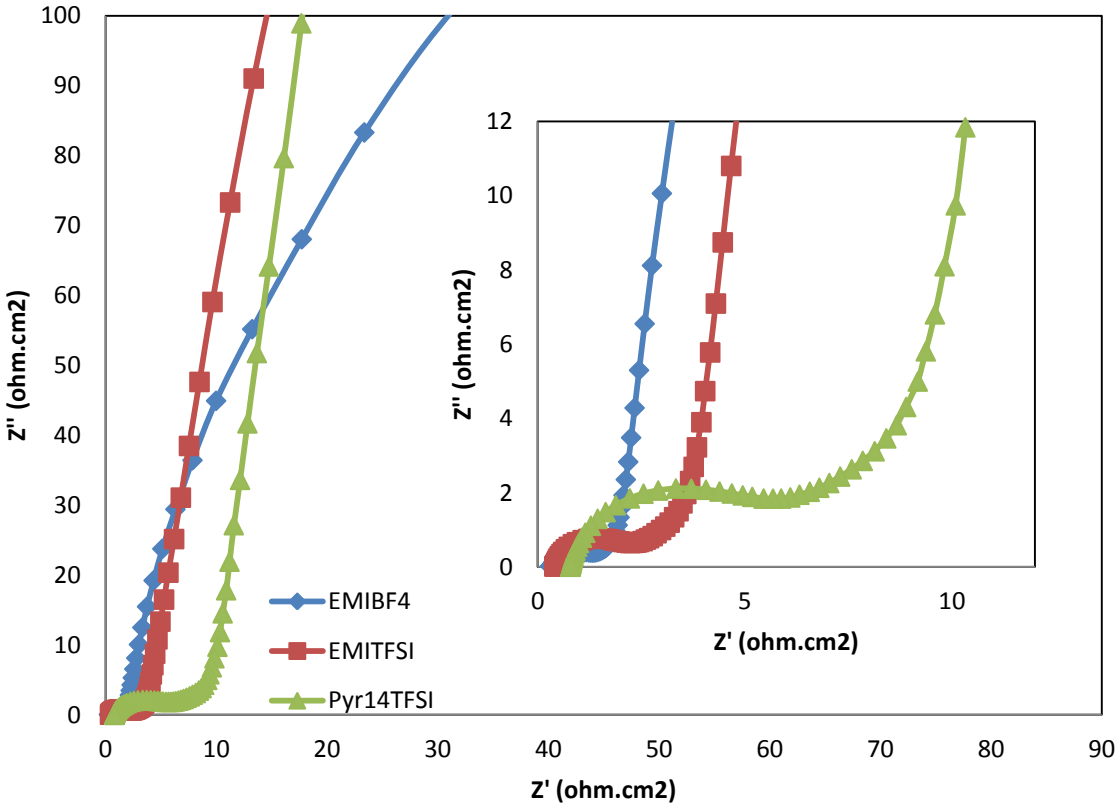

Figure 4.12 Nyquist plots of different pure ionic liquids

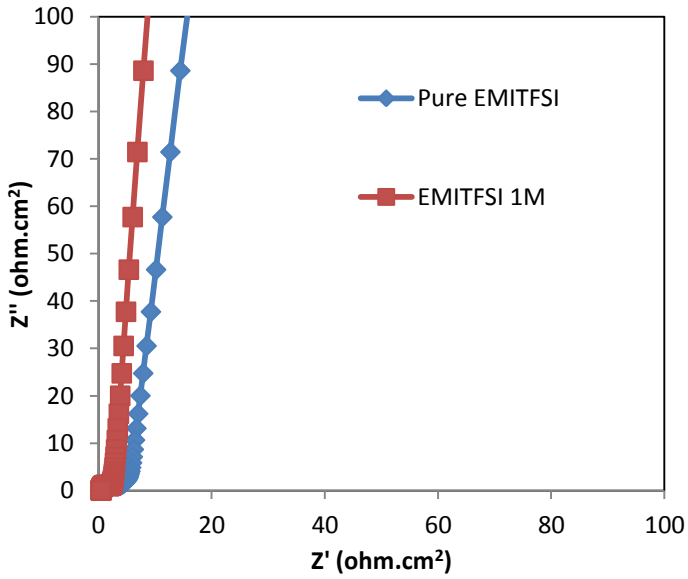

Figure 4.13 Nyquist plots of EMITFSI with and without PC solvent

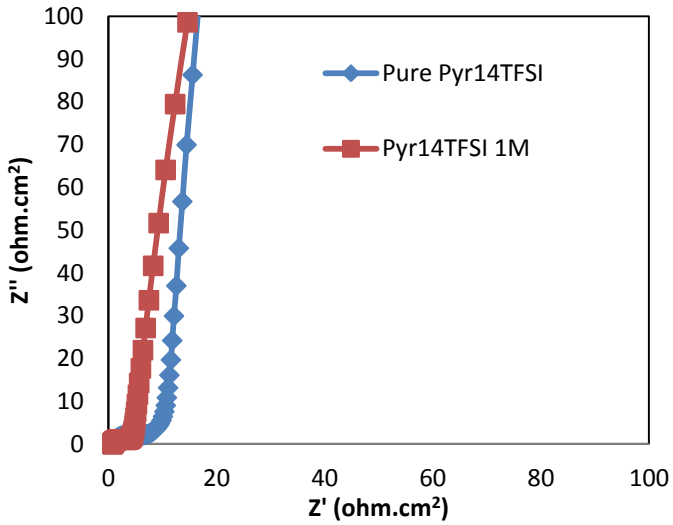

Figure 4.14 Nyquist plots of $Pyr_{14}TFSI$ with and without PC solvent

The real part capacitance (C') is another way to analyze capacitive behaviors of the cells from impedance. From Figure 4.15, all three pure ionic liquid samples showed nicely capacitive behavior that charge ions were stored in the mid range of frequency and then started to reach full capacitance in low frequency around 0.1 Hz and beyond. The trend of real capacitance part is consistent with specific capacitance values from both CV and galvanostatic tests. $EMIBF_4$ still have the best capacitive performance among ionic liquid samples.

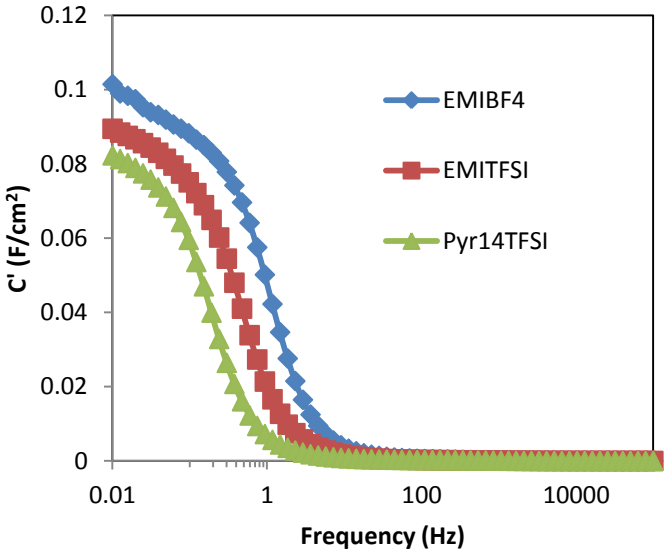

Figure 4.15: Real capacitance part from impedance of each pure ionic liquid samples

The comparison speed of energy storage and delivery of supercapacitor devices can be represented in the term of imaginary capacitance (C'') from EIS [50]. The charismatic time constants calculated from knee or peak frequency for each ionic liquid sample are quite distinguished as shown in Figure 4.16. For $EMIBF_4$, time constant is 1.08 s. For EMITFSI, time constant is 2.65 s. For $Pyr_{14}TFSI$, time constant is 6.58 s. This result could be concluded that small ion sizes and high ionic mobility properties provide fast charge-discharge energy behavior [53]. For EMITFSI/PC and $Pyr_{14}TFSI$/PC, the time constant is decreased to be 1.07 s and 2.11 s respectively. This result means that PC supports ionic liquid ions to increase rate of energy storage mechanism

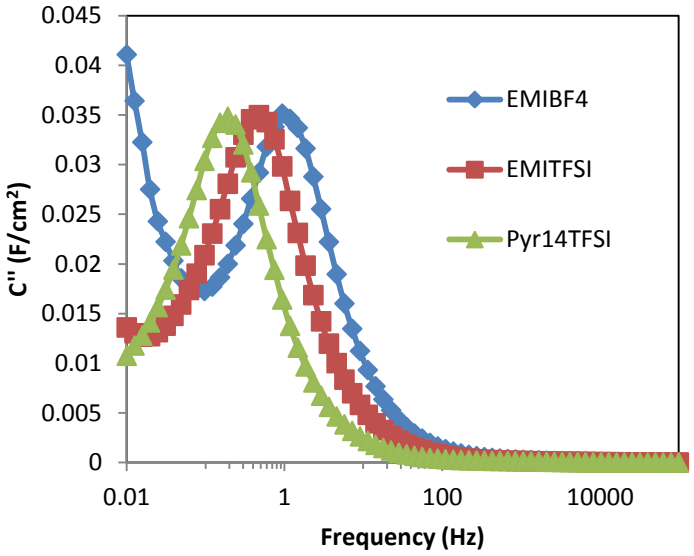

Figure 4.16: Real capacitance part from impedance of each pure ionic liquid samples

4.4 Capacitance Retention: Electrolytes

1000 galvanostatic cycles of each ionic liquid sample were tested to examine capacitance stability of the cells. It turned out as shown in figure 4.17 that $Pyr_{14}TFSI$ maintains the highest stable capacitance about 95.2% following with EMITFSI (92.14%) and $EMIBF_4$ (90.85%). The

reason behind this result is believed that large ion size of $Pyr_{14}TFSI$ have less penetrating and propagating activity on the pores of electrode surfaces. Then, the electrodes have less deformation and still maintain stable capacitive behavior [61].

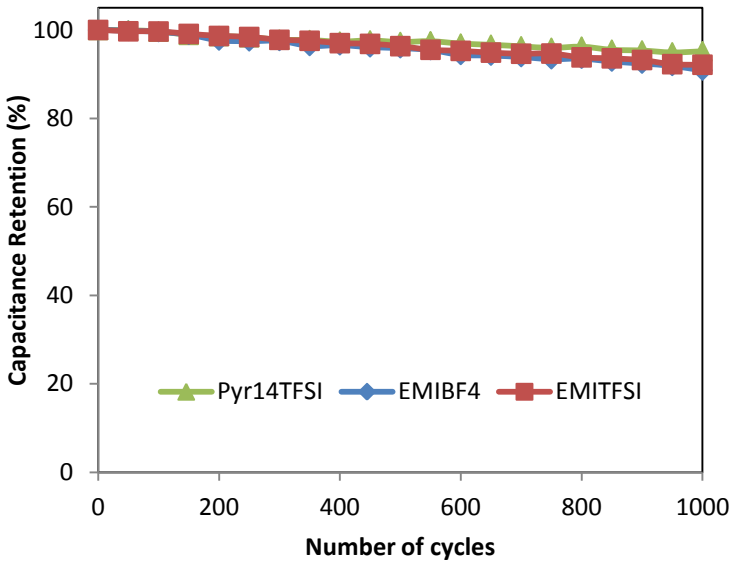

Figure 4.17 Capacitance retention of coated PEDOT/A-CNT 1000 cycles from different pure ionic liquids

4.5 Coulombic Efficiency: Electrolytes

Coulombic efficiency (Eff) also depends on types of electrolyte. The results of Eff for each electrolyte are listed in Table 4.1. $Pyr_{14}TFSI$ have the lowest Eff amount other ionic liquids because big ions that inserted and propagated on polymer coating are more likely to stick in polymer structure and cause the irreversible charge storage. Effs from QV curves that are conversed from CV are different from QV by galvanostatic conversion (Figure 4.18 and Figure 4.19). From CV at scan rate 100 mV/s, $EMIBF_4$ show the highest loss and current leakage than other two electrolytes. However, from galvanostatic test at 0.5 A/g discharge rate, $EMIBF_4$ show the best coulombic efficiency because different electrolytes behave differently at different

frequencies as shown in the loss as a function of frequency from EIS Figure 4.20. The optimal coulombic efficiency can be reached with the right frequency.

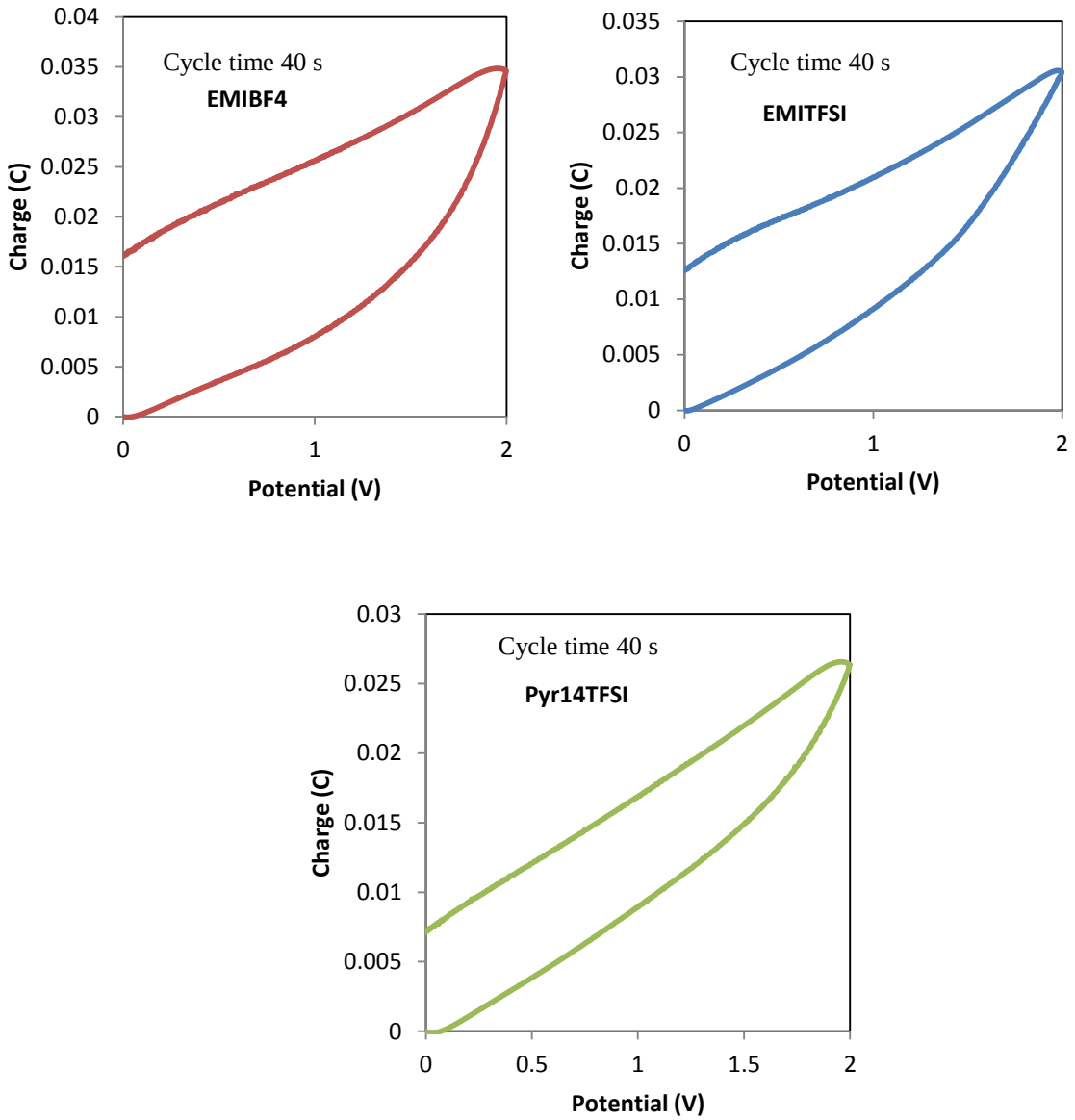

Figure 4.18: QV curves of each electrolyte sample from CV at scan rate 100 mV/s

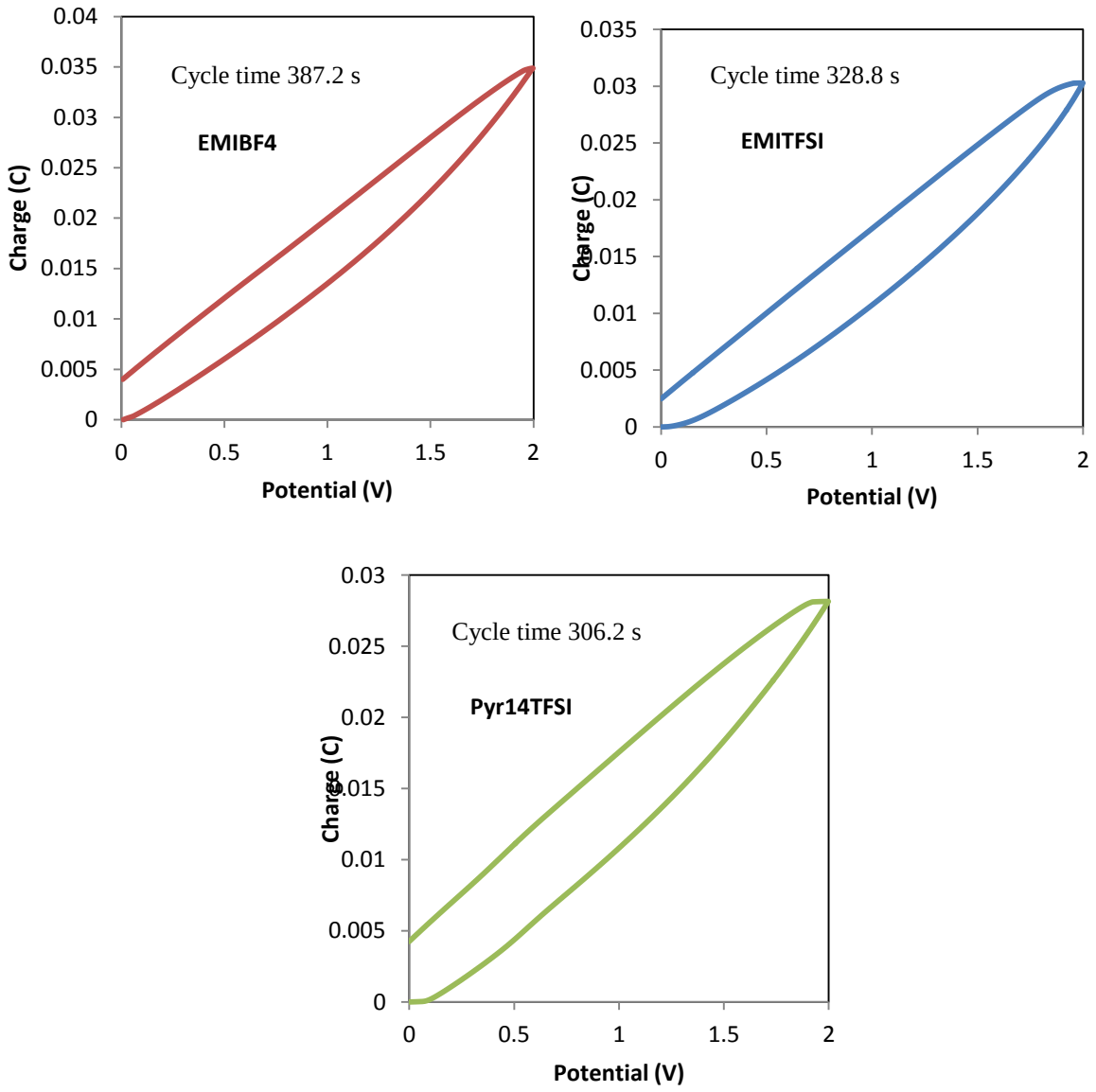

Figure 4.19: QV curves of each electrolyte sample from galvanostatic at charge-discharge rate 0.5 A/g

Electrode	% Efficiency (from Capacitance at 0.5 A/g)	% Efficiency (from Figure 4.18)	% Efficiency (from Figure 4.19)
EMIBF4	91.18	45.26	86.25
EMITFSI	88.89	65.48	85.57
Pyr14TFSI	85.71	78.89	82.41

Table 4.1: Coulombic Efficiency of each electrolyte sample

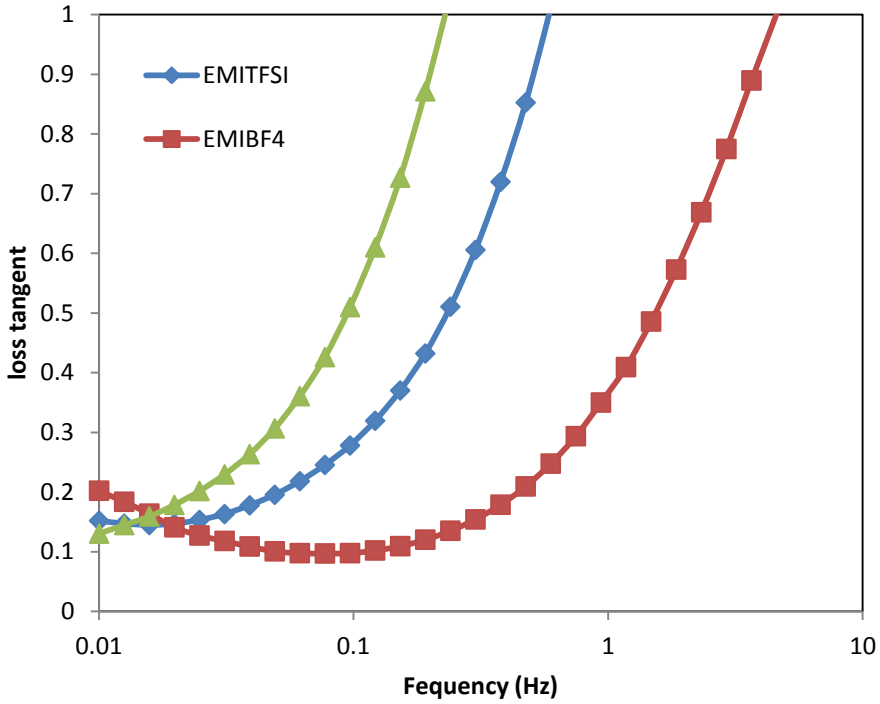

Figure 4.20: loss vs frequency from C'' and C' in EIS of each electrolyte sample

Chapter 5

Conclusion and Future Work

5.1 Conclusion

PEDOT conformal coating has been proved in chapter 3 of this study that it can enhance both power density and energy density especially per unit volume to supercapactor cells with A-CNT electrodes. PEDOT coating not only provides pseudo-capacitance but also provides good conductive properties to induce faster ion propagation. The conformal coating of PEDOT is compatible with the aligned structure, so PEDOT has less mechanic failure compared with coated random CNT samples and then the maximum operating voltage is extended up to 2.0 V. Moreover, the densification of electrodes gives even better performance in volumetric measurement. Therefore, 5% PEDOT/A-CNT is the best performing electrodes in this study. Then, in chapter 4, the electrolyte effect has been investigated to produce higher performing supercapacitors. The results show that ion sizes of ionic liquids have an impact on energy density of the device. The small size ions can propagate on electrode surface area more than bigger size ions. Thus, more propagation leads to higher capacitance values. $EMIBF_4$ has both smallest cations and anions, so it produces the highest capacitance and energy density values. However, the low propagation activity of bigger ions on electrodes makes for better cycle life stability. Besides, the electrolytes with fast ion migration properties such as high ionic conductivity, low viscosity and high ion dissociation could provide high power density. The molecular solvent like PC improves ion migration properties of ionic liquids, so a faster ion migration of the mixture leads to higher power density values. This Ragone plots in Figure 5.1 summarizes the best

performing cells in this study (5% PEDOT/A-CNT with $EMIBF_4$/PC) compared with other kinds of supercapacitors in literatures.

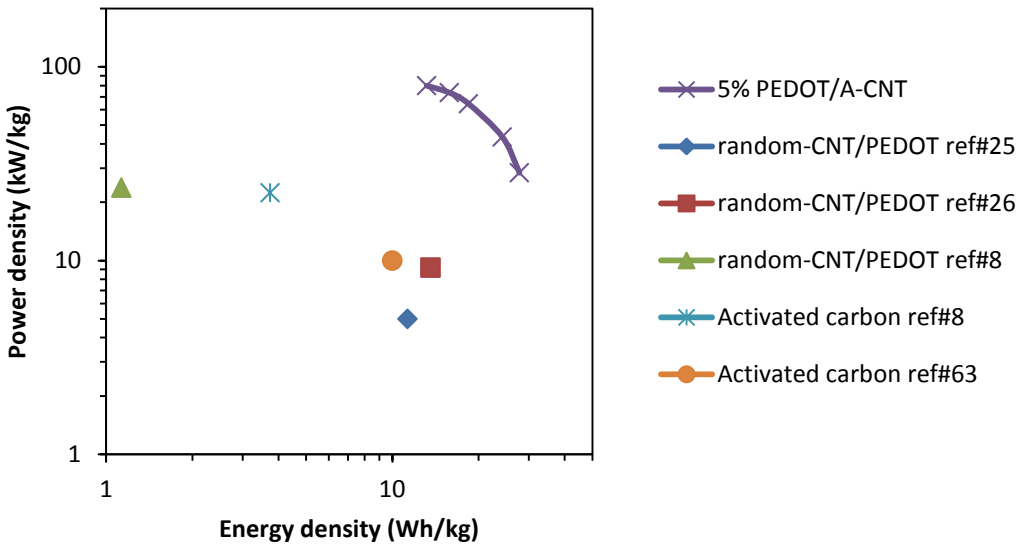

Figure 5.1: Ragone plot summary of this study compared with some literature values

5.2 Future work

Future research will focus on asymmetric and hybrid supercapacitors. The combination of different positive and negative electrodes could extend the operating electrochemical potential and capacitance of the asymmetric supercapacitor devices [62]. Moreover, using some redox reactions as in hybrid batteries could provide more energy density while still keep power density high. Other various types of electrodes such as graphene, metal oxides and other composites could be chosen and investigated to find a highly stable specific capacitance for supercapacitors [9]. Electrolyte also plays a significant role in supercapacitors. New ionic liquids and organic solvents which have compatible ion size with electrodes, high conductivity, low viscosity, and wide operating voltage and temperature could be introduced as well [36].

Reference

1.) M. S. Halper, J. C. Ellenbogen, "Supercapacitor: A Brief Overview" (MITRE Corperation, Mclean, Virginia, 2006).

2.) P. Jampani, A. Manivannan, P. N. Kumta, *Electrochem. Soc. Interface*, 57-62 (2010)

3.) C.Peng, S. Zhang, D. Jewell, G. C. Chen, *Prog. Nat. Sci.* **18**, 777 (2008).

4.) J. Miller, "A Brief history of supercapacitors" (Batteries & Energy Storage Technology, 2007).

5.) D. K. Ariyanayagam, thesis, McMaster University (2011).

6.) B.E. Conway, *Electrochemical Supercapacitors: Scientific Fundamentals and Technological Applications* (Kluwer Academic/Plenum Publishers, New York, 1999).

7.) A. G. Pandolfo, A.F. Hollenkamp, *J. Power Sources* **157**, 11-27 (2006).

8.) E. Frackowiak, *Phys. Chem. Chem. Phys* **9**, 1774-1785 (2007).

9.) G.Wang, L. Zhang, J. Zhang, *Chem. Soc. Rev.* **41**,797-828 (2012).

10.) Y. Wang et al., *J. Phys. Chem.* **113**, 13103-13107 (2009).

11.) P. Simon, Y. Gogotsi, *Acc. Chem. Res.* **46** (5), 1094-1103 (2013).

12.) D.N. Futaba et al., *Nat. Mater.* **5**, 987-994 (2005).

13.) B. L. Wardle et al., *Adv. Mater.* **9999**, 1-8 (2008).

14.) H. Zhang, G. Cao, Y. Yang, Z. Gu, *J. Electrochem. Soc.* **155** (2), K19-K22 (2008).

15.) P. Simon, Y. Gogotsi, *Nat. Mater*. **7**, 845-854 (2008).

16.) W. Wei, X. Cui, W. Chen, D. G. Ivey, *Chem. Soc. Rev.* **40**, 1697-1721 (2011).

17.) Q. Cheng, J. Tang, J. Ma, H. Zhang, N. Shinya, L.-C. Qin, *Carbon* **49**, 2917-2925 (2011).

18.) L. Nyholm, G. Nyström, A. Mihranyan, M. Strøme, *Adv. Mater.* **23**, 3751-3769 (2011).

19.) G. A. Snook, P. Kao, A. S. Best, *J. Power Sources* **196**, 1-12 (2011).

20.) C. Peng, S. Zhang, D. Jewell, G. Z. Chen, *Prog. Nat. Sci.* **18**, 777-788 (2008).

21.) D. K. Bhat, M. S. Kumar, *J. Mater. Sci.* **42**, 8158-8162 (2007).

22.) Y. Zhou, Y. Liu, *M. Ghaffari*, M. Lin, E. Parsons, B. L. Wardle, Q. M. Zhang, *J. Power Sources*, in press (2012).

23.) J. Wang, Y. Xu, X. Sun, X. Li, *J. Solid State Electrochem.* **12**, 947-952 (2008).

24.) E. Frackowiak, V. Khomenko, K. Jurewicz, K. Lota, F. Béguin, *J. Power Sources* **153**, 413-418 (2006).

25.) X. Bai et al., *Electrochim. Acta*, **87**, 394-400 (2013).

26.) P. J. Kulesza, M. Skunik, B. Baranowska, M. Chojak, K. Miecznikowski, *J. Electrochem. Soc.* **6** (25), 245-256 (2008).

27.) K. Lota, V. Khomenko, E. Frackowiak, *J. Phys. Chem. Solids* **65**, 295-301 (2004).

28.) D. Antiohos et al., *J. Mater. Chem*. **21**, 15987-15994 (2011).

29.) M. D. Stoller, R. S. Ruoff, *Energy Environ. Sci*. **3**, 1294–1301 (2010).

30.) J. L. Bideau, L.Viau, A.Vioux, *Chem. Soc. Rev.* **40**, 907-925 (2011).

31.) J.-P. Belieres, C. A. Angell, *J. Phys. Chem. B* **111**, 4926–37 (2007).

32.) H. Ohno, *Electrochemical Aspects of Ionic Liquids* H. Ohno, Ed. (John Wiley & Sons, Inc., Hoboken, New Jersey 2005).

33.) A. Krause, A. Balducci, *Electrochem. Commun.* **13**, 814-817 (2011).

34.) M. Biso, M. Mastragostino, M. Montanino, S. Passerini, F. Soavi, *Electrochim. Acta* **53**, 7967-7971 (2008).

35.) A. Balducci, W. A. Henderson, M. Mastragostino, S. Passerini, P. Simon F. Soavi, *Electrochim. Acta* **50**, 2233-2237 (2005).

36.) L.E. Barrosse-Antle *et al.*, *Chem. Asian. J.* **5**, 202-230 (2010)

37.) M. Montanino, M. Carewska, F. Alessandrini, S. Passerini, G. B. Appetecchi, *Electrochim. Acta* **57**, 153-159 (2011).

38.) R. Taniki, K. Matsumoto, R. Hagiwara, *Electrochem. Solid-State Lett.* **15** (4), F13-F15 (2012).

39.) P. Johansson, L. E. Fast, A. Matica, G. B. Appetecchib, S. Passerini, *J. Power Sources* **195**, 2074-2076 (2010).

40.) A. Balducci, F. Soavi, M. Mastragostino, *Appl. Phys. A.* **82**, 627-632 (2006).

41.) M. Chai, Y. Jin, S. Fang, L. Yang, S.-I. Hirano, K. Tachibana, *J. Power Sources* **216**, 323-329 (2012).

42.) K. Liu et al., *Electrochim. Acta* **55**, 7145-7151 (2010).

43.) H.-B. Han et al., *Electrochim. Acta* **55**, 7134-7144 (2010).

44.) M. Kunze et al., *J Phys. Chem. C* **115**, 19431-19436 (2011).

45.) P. Dvořák, "Overview of Non-aqueous Electrolytes for Supercapacitors" (FEEC BUT 2010).

46.) Y. Zhou et al., "Asymmetric Supercapacitor Based on PEDOT/A-CNTs and Nanoporous Graphene with High Volumetric Power and Energy Density" (Accepted *Adv.Mater.* 2013).

47.) E. I. Rogers *et al.*, *J. Chem. Eng.*, **54**, 2049-2053 (2009).

48.) G. H. Lanes, *Electrochim. Acta*, **83**, 513-529 (2012).

49.) S. Vaddiraju, H. Cebeci, K. K. Gleason, B. L. Wardle, *ACS Appl. Mater. Interfaces* **1** (11), 2565-2572 (2009).

50.) M. Ghaffari, Y. Zhou, H. Xu, M. Lin, R. S. Ruoff, Q. M. Zhang, "High Volumetric Performance Aligned Nano-Porous Graphene-based Electrochemical Capacitors" (Accepted *Adv.Mater.* 2013).

51.) Y. Zhou, Y. Liu, *M. Ghaffari*, M. Lin, E. Parsons, B. L. Wardle, Q. M. Zhang, *J. Power Sources*, in press (2012).

52.) S. Liu, Y. Liu, H. Cebeci, R. G. Villoria, J. H. Lin, B. L. Wardle, Q. M. Zhang, *Adv. Funct. Mater.* **20**, 3266-3272 (2010).

53.) P. L. Taberna, P. Simon, J. F. Fauvarque, *J. Electrochem. Soc.***150** (3), A292-A300 (2003).

54.) W. Lua, L. Qub, K. Henrya, L. Dai, *J. Power Sources*, **189,** 1270–1277 (2009).

55.) Y. Liu, dissertation, Pennsylvania State University (2012).

56.) A. Balducci, R. Dugas, P.L. Taberna , P. Simon, D. Pl´ee, M. Mastragostino, S. Passerini, *J. Power Sources* **165**, 922-927 (2007).

57.) J. Segalini, E. Iwama, P.-L. Taberna, Y. Gogotsi, P. Simon, *Electrochem. Commun*. **15** , 63–65 (2012).

58.) C. Largeot, P. L. Taberna, Y. Gogotsi, P. Simon, *Electrochem. Solid-State Lett.* **14** (12), A174-A176 (2011).

59.) C. Largeot, C. Portet, J. Chmiola, P.-L. Taberna, Y. Gogotsi, P. Simon, *J. Am. Chem. Soc.* **130**, 2730-2731 (2008).

60.) F. B. Sillars, S. I. Fletcher, M. Mirzaeian and P. J. Hall, *Phys. Chem. Chem. Phys*. **14**, 6094–6100, (2012).

61.) R. Lin et al., *Electrochim. Acta* **54**, 7025–7032 (2009).

62.) Khomenko, V.; Raymundo-Piñero, E.; Frackowiak, E.; Béguin F. *Appl. Phys. A* **82**, 567-573 (2006).

63.) L. L. Zhang, X. S. Zhao, *Chem. Soc. Rev.* **38**, 2520–2531 (2009).